HYPERLYNX

FINAL REPORT

Prepared by: Connor Catterall, Ben Cooper, Nicole Garcia, George Kemp, Chandler Lacy, John Spinelli, Mark Urban, and Susan Waruinge

12/3/2015

ABSTRACT

In the summer of 2015, Team HyperLynx was one of over three hundred collegiate teams to initially enter the SpaceX Hyperloop pod competition. Now, Team HyperLynx is one out of the hundred teams remaining in the competition, and will present a final design package at Texas A&M University to industry engineers. Teams that progress to the next competition phase will present complete pod builds to be tested in a half-scale test track at SpaceX headquarters in California. This report outlines the Team HyperLynx design package to manufacture a functional, half-scale Hyperloop pod that will be accelerated at 2.4g's to 240 mph inside the SpaceX launch tube. The pod will interface to a 1-mile long, 6-foot outer diameter, steel tube resting above ground on concrete pylons. Inside, concrete fills the tube bottom to a depth of six inches. The concrete creates a flat surface that supports a 6061-T6 Aluminum subtrack, two 15 inch flat plates separated by a central I-beam (6 in. width, 4 in. height). The tube will be evacuated to 0.02 psi to dramatically reduce system drag. Finally, the test track features an accelerating pusher cart that launches pods to maximum speed over an 800 foot acceleration section at the beginning of the track. The purpose of the launch is to test system designs. A successful pod will launch to maximum speed, record and transmit all available flight data, and complete a stop sequence that damages neither the pod nor the test track.

The Team HyperLynx Hyperloop pod is an Aluminum frame, carbon fiber shelled, magnetically levitated payload delivery system. The pod is 14 feet in length, approximately 3 feet at max width and 3 feet at max height, and has an estimated weight of 1000 lbs. The system will deliver a 72 VDC battery power plant, an embedded control system that alters

and records flight characteristics, an environmental (temperature, pressure, vibration) data logging system, a test flight dummy, braking system, and chassis through the test track using onboard magnetic levitation. Although choked flow will not occur in the SpaceX test track due to low (less than Mach 0.3) speeds, the pod will feature a ducted fan to showcase options for dealing with drag at speeds near the speed of sound. This document represents a tentative final design package for the HyperLynx pod. Several aspects detailed in this report are subject to change. For example, Team HyperLynx believes it can reduce total pod weight by over 50% by eliminating non-load bearing members from the frame and reducing shell thickness, while still maintaining safety factors of 2. Team HyperLynx aims to win the SpaceX pod competition by developing a functioning, lightweight, and practical pod design. Furthermore, the team desires to donate its work and efforts to contribute to the development of a working, full scale Hyperloop system.

Contents

1 INTRODUCTION

In 2014, the airline industry in the United States served over 850 million passengers. This number consistently grows each year as more people take to the skies. This leads to overbooked flights, crowded airplanes, and an increase in overall travel cost. There is a growing demand for transportation alternatives that can provide consumers with safer, cheaper and faster travel. The Hyperloop offers the next step in innovation. The Hyperloop aims to reduce the cost of transportation, eliminate the dependency on fossil fuels, and decrease travel time. The Hyperloop transportation system consists of pods traveling inside low-pressure steel tubes at speeds over 700 mph, near the speed of sound. The pod will achieve near frictionless travel by employing magnetic levitation to eliminate contact between the tube and the pod. Figure 1 shows a conceptual rendering of the pod traveling inside the tube.

Figure 1. Rendering of Hyperloop Pod

The idea of rapid tube transport can be traced back to 1951 when Robert Goddard patented a system of pods and tubes to transport people. More recently, companies such as SpaceX, ET3 and Hyperloop Transportation Technologies have tried to develop Goddard's idea into a feasible transportation system by building scale models and performing feasibility studies. More specifically, Elon Musk of SpaceX initially proposed the concept of the Hyperloop in August 2013. This was in response to the approval of the California high-speed rail which would be, as Musk states in his Hyperloop white paper, "[o]ne of the most expensive per mile and one of the slowest in the world." Musk proposed the Hyperloop as an alternative to high-speed rail traveling between Los Angeles and San Francisco, a distance of approximately 380 miles as shown in Figure 2. The Hyperloop aims to cut travel time between the two cities ten fold, allowing passengers to travel between Los Angeles and San Francisco in 30 minutes.

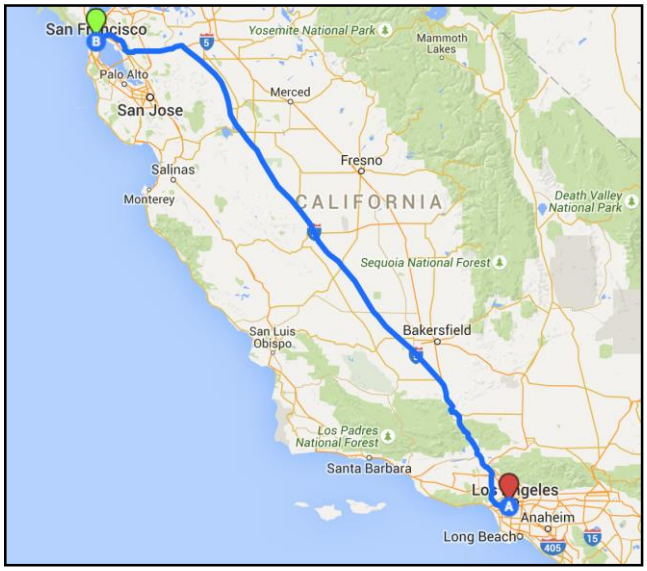

Figure 2. Proposed Hyperloop Route (Photo courtesy of Google Maps)

To drive innovation and development of the Hyperloop, SpaceX will host a competition showcasing a half scale Hyperloop transportation system. College teams around the country will design and develop a working Hyperloop Pod while SpaceX will build a tube to test the pods. The competition will utilize an open-sourced information strategy to drive the development of a prototype Hyperloop system.

The goal of Team HyperLynx is to design and manufacture a prototype Hyperloop pod, which will travel at speeds over 200 mph. More specifically, Team HyperLynx aims to design the fastest and the lightest pod possible. The prototype design will address the challenges that set this concept apart from current modes of transportation such as the environment, speed and economic viability.

The Hyperloop concept can be divided into 9 major subsystems: aerodynamics, frame, body, levitation, internal flow, propulsion, controls, power, and safety. The body of the pod will reduce drag inside the tube and will be constructed out of carbon fiber. The frame will

support the body and provide mounting for any subsystem components. The frame will be constructed out of carbon fiber and aluminum. Inside the pod, the internal flow system will pass incoming air through the pod, further decreasing drag. The levitation system will consist of 6 levitating engines that will suspend the pod on a magnetic field. A wheeled vehicle inside the tube will interface with the back of pod, providing propulsion. Each subsystem will be connected using a control system. A skeleton view and an exploded view showcasing each subsystem are shown in Figure 3.

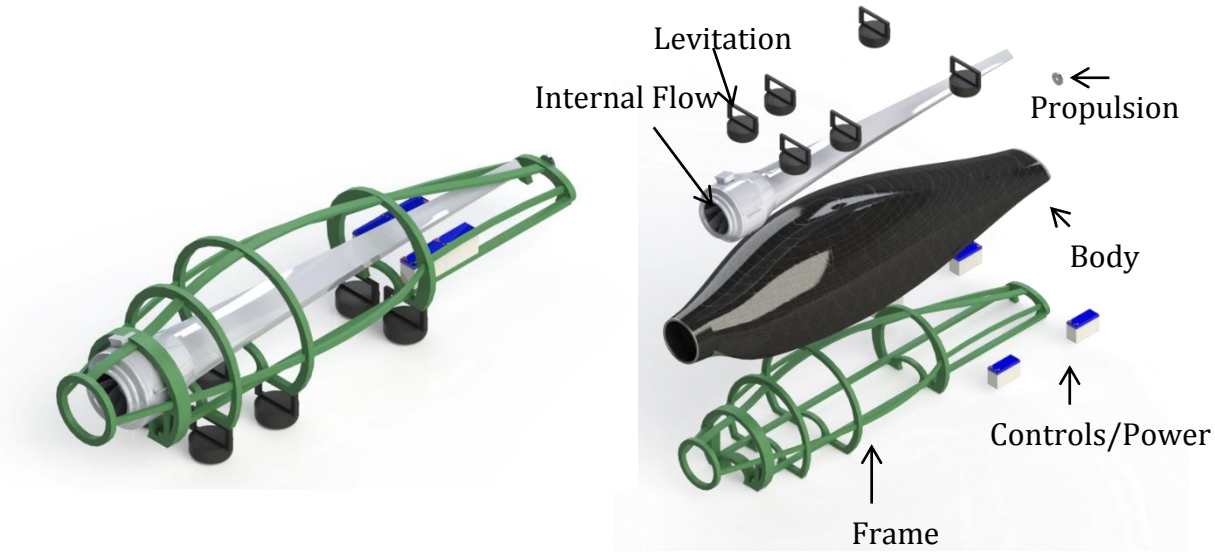

Figure 3. Skeleton and Exploded view of Hyperloop Pod

This report details the overall pod design, pod sub-system specifications, future plans and an estimated construction timeline.

2 AERODYNAMICS

Choked Flow Analysis

One of the primary design challenges of the Hyperloop is overcoming choked flow that the pod will encounter when it travels at high speeds through a tube. To circumvent this

problem, the HyperLynx prototype pod will incorporate an axial fan and ducting system to redirect air from air traveling around the pod and propel it through the pod.

Determining the mass flow rate of air within the tube that will cause choked flow is key to designing the fan. Choked flow occurs when air traveling past the pod reaches Mach 1 and it happens at the area of minimum cross-sectional flow. To calculate the choked flow rate, first the total upstream mass flow rate in the tube must be determined. This value is based on the cross-sectional area of the tube A_{Tube} and the Mach speed of the pod M. The cross-sectional area of the tube is calculated to be $A_{Tube} = 2.51846\ m^2$ from the dimensions shown in Figure 4.

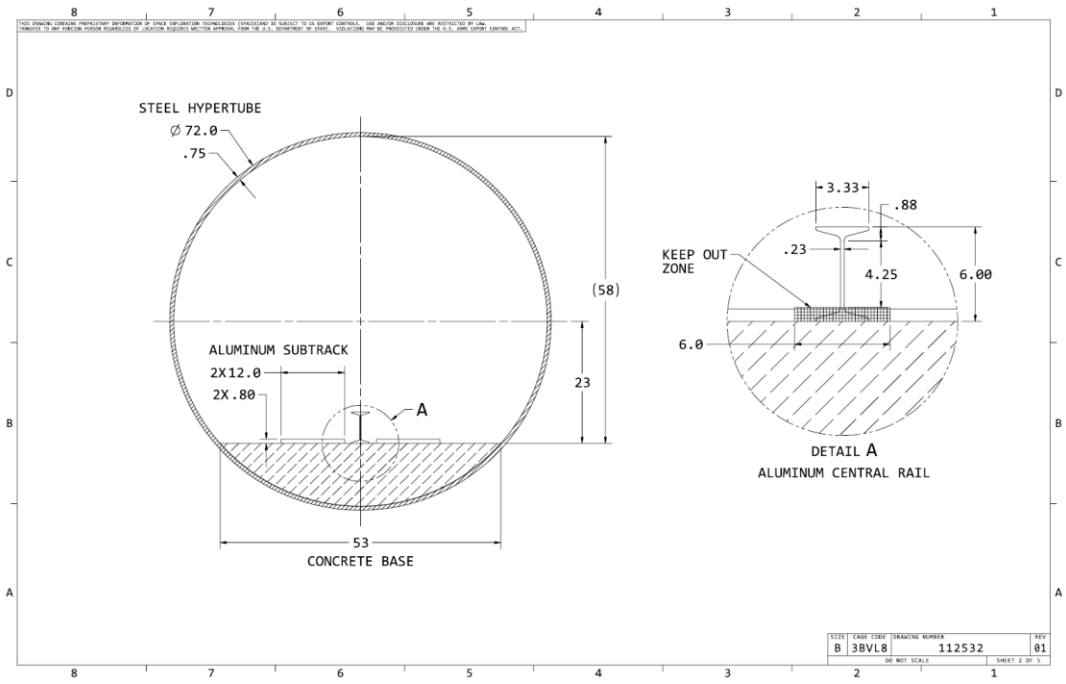

Figure 4. Hyperloop Test Track Dimensions

The total upstream mass flow rate is calculated by the following:

$$m_T = \frac{A_{Tube} P_t}{\sqrt{T_T}} \sqrt{\frac{\gamma}{R}} M\left(1 + \frac{\gamma - 1}{2} M^2\right)^{-\frac{\gamma+1}{2(\gamma-1)}} \qquad \textit{Equation 1}$$

where P_t is the stagnation pressure, T_T is the stagnation temperature, M is the mach number of the pod, γ is the specific heat capacity of air, and R is the gas constant of air. Figure 5 shows the upstream mass flow rate as a function of pod velocity. These calculations were done assuming a 130Pa system at room temperature.

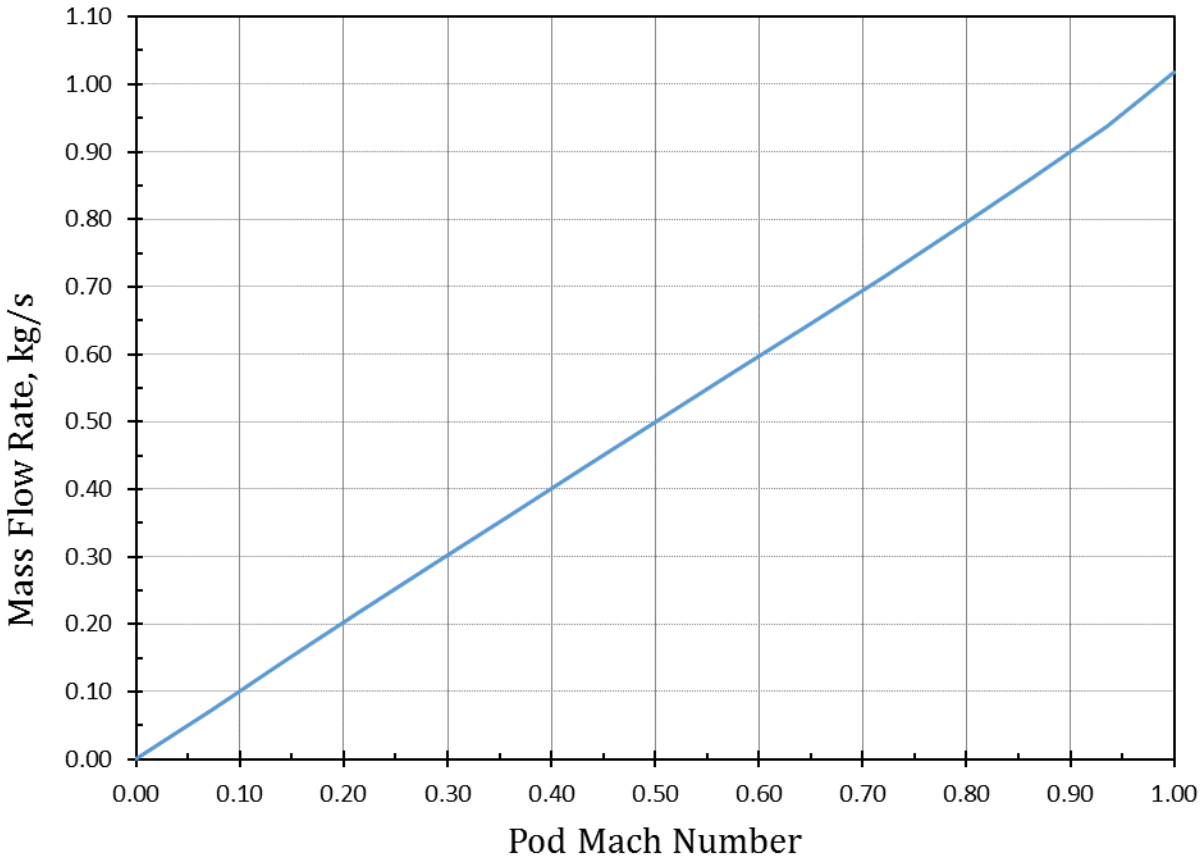

Figure 5. Upstream Mass Flow Rate within Test Track

This mass flow rate information is essential to determining the choked flow rate. Choked flow will occur where the cross-sectional area around the pod reaches a minimum. This area is where the pod cross-sectional area is the maximum. The difference between the tube cross-sectional area and the pod cross-sectional area, A_{Choked}, is used to calculate the choked mass flow rate as follows:

$$m_{Choked} = \frac{A_{Choked} P_t}{\sqrt{T_T}} \sqrt{\frac{\gamma}{R}} \left(\frac{\gamma-1}{2}\right)^{-\frac{\gamma+1}{2(\gamma-1)}} \qquad \textit{Equation 2}$$

Based upon the preliminary dimensions of the pod, $m_{Choked} = .558\ kg/s$. With the choked mass flow rate and upstream mass flow rate known, the mass flow rate that the fan must induce can be calculated in $m_{Fan} = m_T - m_{Choked}$ Equation 3.

$$m_{Fan} = m_T - m_{Choked} \qquad \textit{Equation 3}$$

Figure 6 shows the mass flow rate that the fan must take in to avoid choked flow. Note that the flow rates shown are the minimum, and the fan should be designed such that it will take in slightly more to ensure that choked flow does not occur.

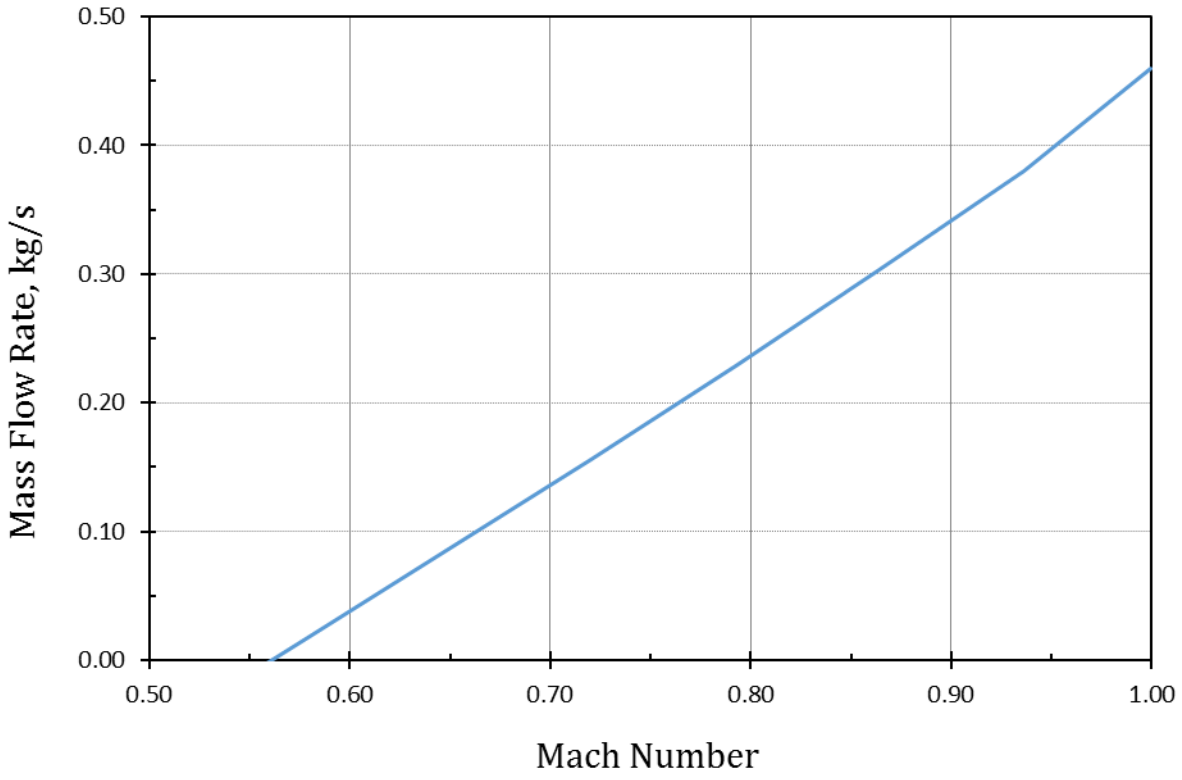

Figure 6. Minimum mass flow rate that the fan must induce to avoid choked flow

Note that below speeds of .55 Mach the fan does not need to intake any air for the purposes of avoiding choked flow. Computational fluid dynamics software was used to run 3-D flow

simulations at various pod speeds to compare to the analytically derived choked flow rate. Simulations for $M = .29$, $M = .43$, $M = .50$, $M = .58$, and $M = .65$ are shown in Figure 7 - Figure 11.

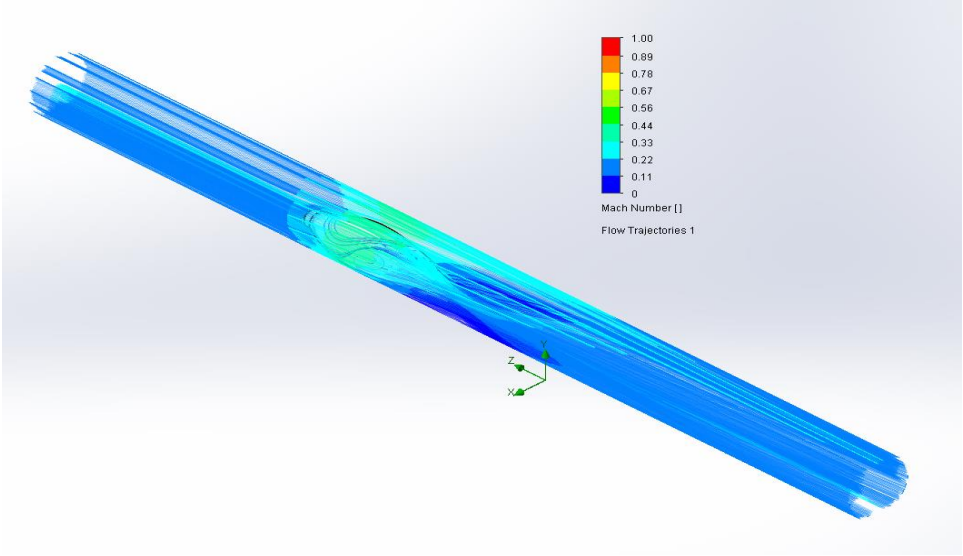

Figure 7. Flow simulation at M=.29

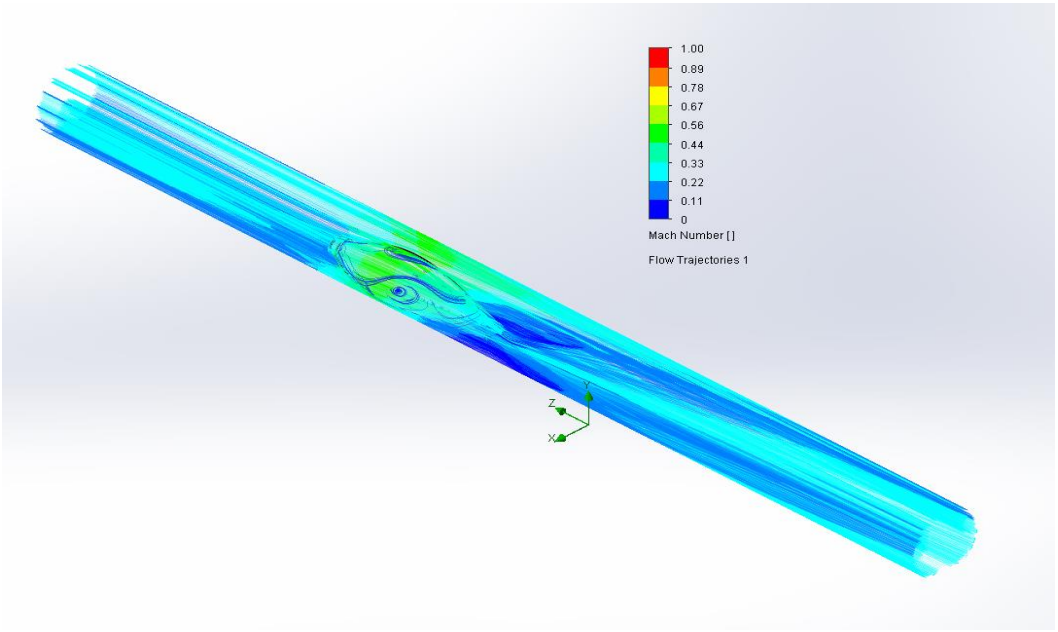

Figure 8. Flow Simulation at M=.43

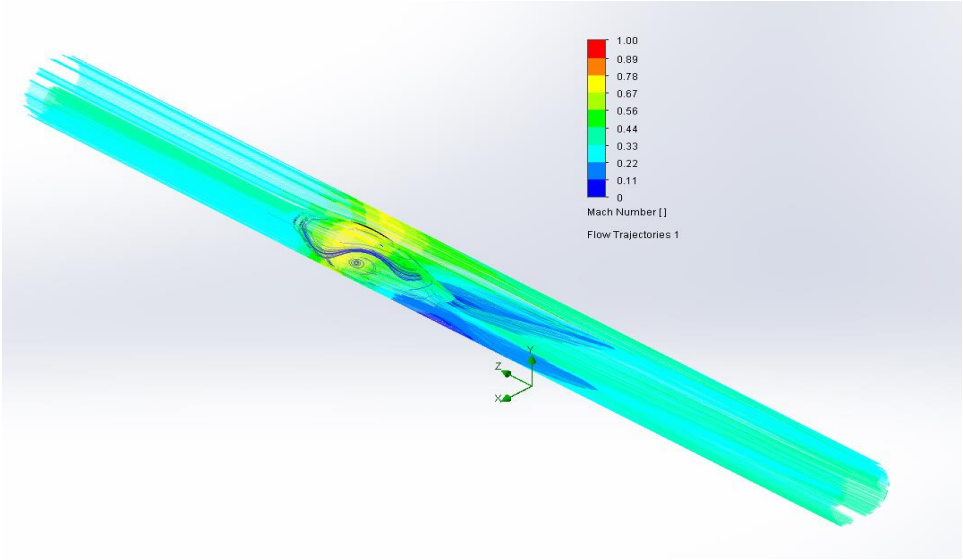

Figure 9. Flow Simulation at M=.5

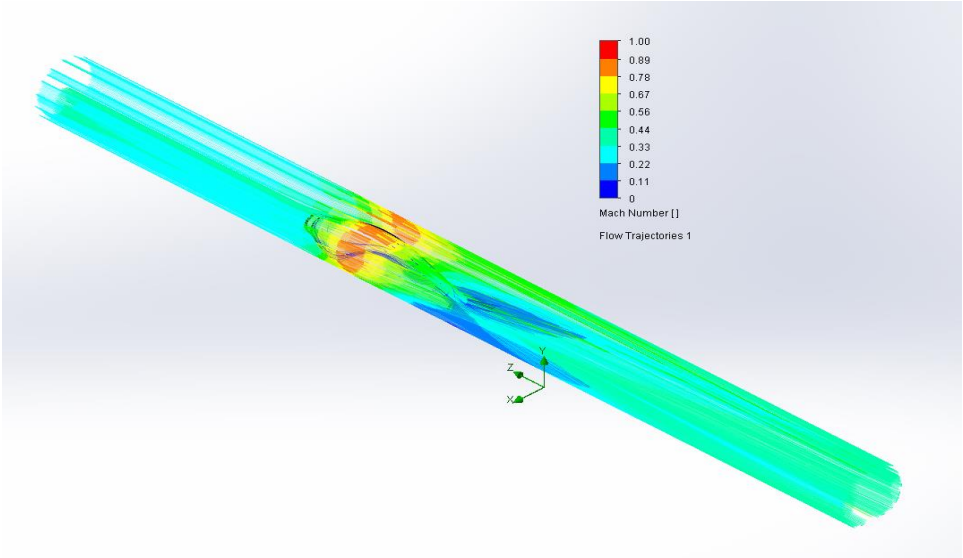

Figure 10. Flow Simulation at M=.58

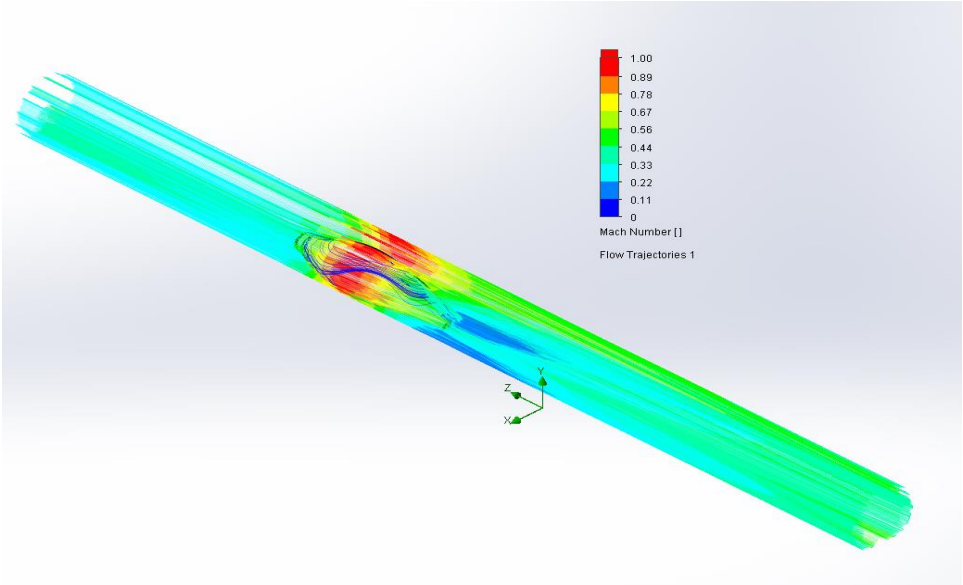

Figure 11. Flow Simulation at M=.65

The previous calculations state that choked flow will occur at $m_{Choked} = .558\ kg/s$. Figure 10 shows that choked flow begins to develop around the pod at $M = .58$. Based upon the simulations shown in

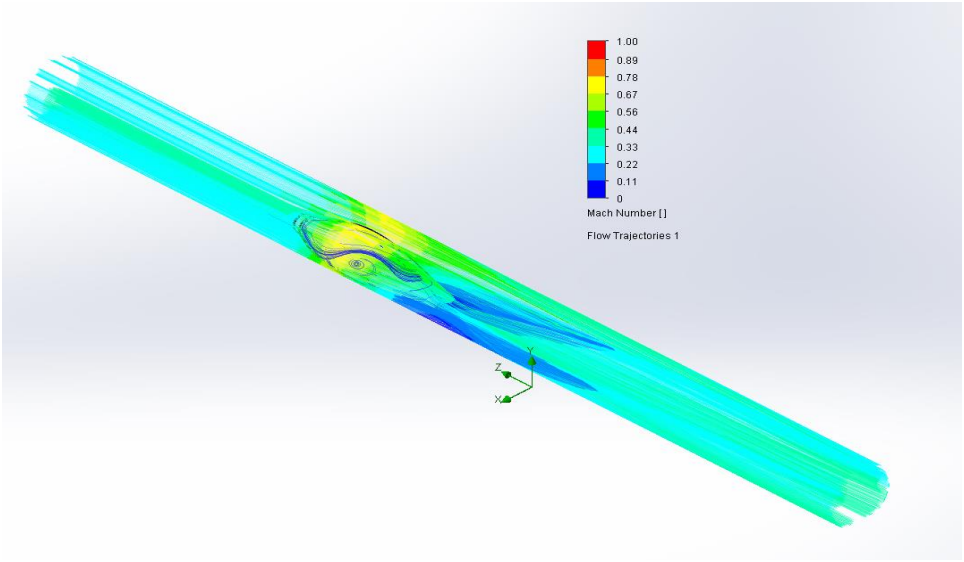

Figure 9 and Figure 10, choked flow will occur when the pod reaches speeds somewhere between $M = .5$ and $M = .58$. Figure 6 shows that choked flow will occur just after $M = .55$.

Due to the limited amount of track available and limitations of the propulsion system, the max speed achievable is Mach .3214, much less than the Mach .55 that would cause choked flow. Thus for the initial testing, the fan is not necessary, however, due to the competition's requirement to show how the pod would be scaled up it will still be included in the overall design to meet the needs of the Hyperloop.

3 POD FREE BODY DIAGRAM

To determine the loading on the pod, a free body diagram was created showing loading from several subsystems and the environment. The free body diagram shown in Figure 12 takes in to account the force from the pusher, the levitation motors, drag, and the weight of the pod. Moments from the levitation motors and the intake fan are coupled together into a moment about the center of gravity. Figure 12 and Figure 13 show the free body diagram of the pod. Table 1. Symbol Definitions shows the forces and labels used in the free body diagram.

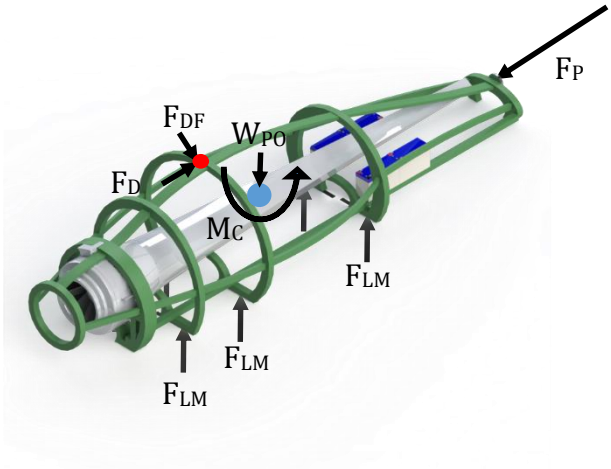

Figure 12. Isometric FBD

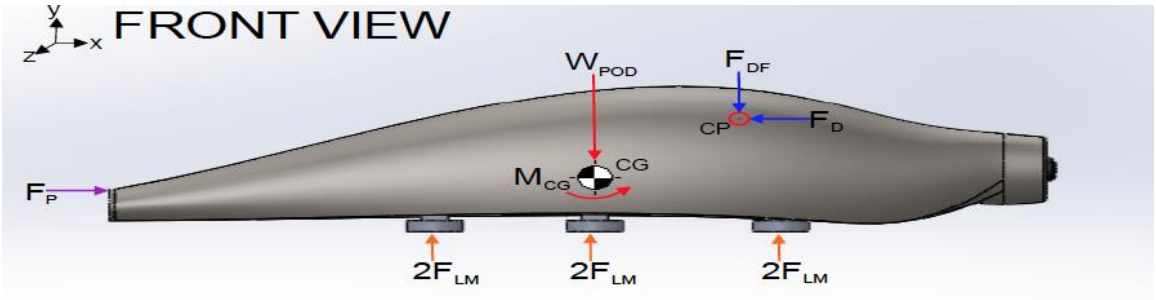

Figure 13. Pod Free Body Diagram

Table 1. Symbol Definitions

Symbol	Definition
F_P	Force of the pusher
F_{LM}	Force of the Levitation Motors
M_{CG}	Moment about the Center of Gravity
W_{POD}	Weight of Pod
F_D	Force of Drag
F_{DF}	Down Force
CP	Center of Pressure
CG	Center of Gravity

4 BODY

The primary focus when designing the body and frame was to offer maximum structural integrity while minimizing weight. At high speeds, the body will keep the payload safe inside the pod and accelerate the air flowing around the pod.

The overall goal of the body design is to minimize the drag on the pod. When unity (that is, Mach 1) is reached inside a tube, the flow is said to be choked. The nozzle geometry at the front of the pod increases the velocity of the air around the maximum height of the pod, while the diffuser allows the high velocity air to expand more rapidly, further decreasing drag. In order to determine the size of the pod, CFD analysis was performed to find the optimal size and shape of the pod. The optimum results of the CFD are shown in Table 2.

Optimum dimensions of pod. These values are defined as a ratio between the dimension and the tube size.

Table 2. Optimum dimensions of pod

Dimension	Length	Height
Value	3.5:1	0.6:1

[place CFD here]

Using these results a body shape was designed that would maximize the efficiency of the pod design. In order to prove its efficiency, the model shown in Figure 14 was printed and tested in the wind tunnel. See the Wind Tunnel Testing section for more information on the testing.

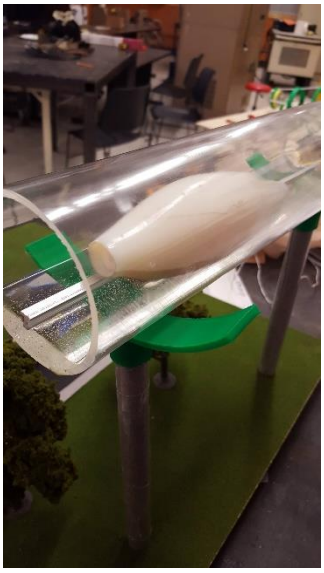

Figure 14. 3D Printed Body Shape

Various body construction techniques have been tested. The body of the pod, like a car or plane, provides a barrier between the environment of the tube and the environment inside the pod. To mitigate the pressure on the body a carbon fiber shell will be constructed

around the pod. Carbon fiber is a lightweight composite that can mold to complex shapes without compromising strength. The next step in the body design is to conduct a study to find the heat distribution around the body while traveling at high speeds and test the carbon fiber construction technique on a small scale.

5 FRAME

The frame of the Hyperloop pod will be modeled similar to the fuselage of an aircraft. The frame will be designed to resist the tension, compression, and bending moments the pod will experience. The overall goal of the frame is to offer structural support to other subsystems such as levitation and the intake fan while minimizing weight. Like an aircraft, the pod will be comprised of formers and stringers. The formers provide the structure for which the body will mount to. The stringers are connected in between the formers and stretch the length of the pod. In addition to the formers and stringers, longitudinal beams on the bottom of the pod will interface with the formers to provide mounting support for the levitating engines and landing gear. The initial frame design can be seen in Figure 15.

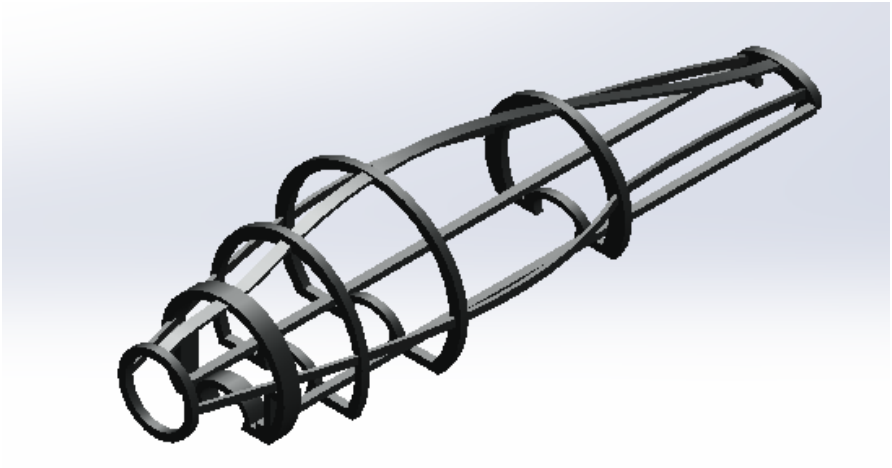

Figure 15. Initial Frame Design

In order to test frame construction, a miniature frame was printed using a 3D printer and assembled. This is shown in Figure 16.

Figure 16. Frame Construction Test

[Add FEA]

6 FAN DESIGN

According to the Air Movement and Control Association, there are four basic parameters required to select a fan. They are:

- Installation Type
- Density at the fan inlet
- Desired airflow rate
- Required pressure

Based upon these parameters a fan manufacturer can size an appropriate fan for the pod. The installation type for the pod will a free inlet and ducted outlet. Air will enter from the tube and travel through ducting that leads out the back of the pod.

The density of air at the inlet is given by the ideal gas law. The desired airflow rate, or volumetric flow rate, is calculated assuming that air is incompressible, which suits the HyperLynx pod because air will not reach speeds above Mach .3. The pressure required to move the airflow rate is the difference between the total pressures at the fan inlet and outlet. This is also called the total fan pressure. This can be calculated by applying Bernoulli's Principle:

$$P_1 - P_2 = \rho(V_2^2 - V_1^2) \qquad \textit{Equation 4}$$

where V_1 and V_2 are velocities at fan inlet and outlet and P_1 and P_2 are the total pressures at fan inlet and outlet. This relationship only holds for constant density.

The airflow rate and total pressure equations above depend on the mass flow rate of air, m_{fan}, that must enter the fan to avoid choked flow around the pod. However, the HyperLynx prototype will not reach speeds high enough to encounter choked flow, meaning the fan is unnecessary for the pod to function. The fan will still be included in the design in the spirit of the overall Hyperloop concept. For this reason, a simple fan that is relatively cheap, lightweight, and easy to mount to the pod was chosen. The fan comes fully equipped with a variable-speed drive and electric motor. This allows the fan to increase speed as the pod travels faster in order to send more air through the pod.

Figure 17. Atmosphere V-16XL Fan

The performance of the fan is based on the static pressure of air. Figure 18 below shows the relationship between static pressure and the airflow rate that the fan induces. Again, the performance of the fan is not critical to the functionality of the HyperLynx pod.

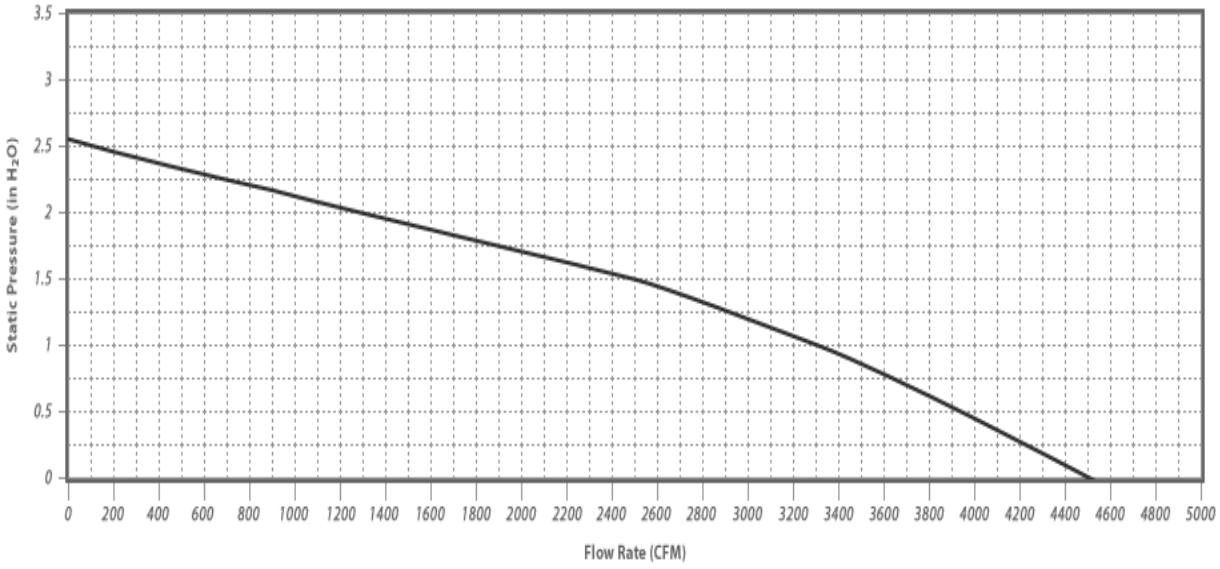

Figure 18. V-16XL Fan Performance Curve

7 PROPULSION

The HyperLynx prototype pod will be accelerated through the tube by a propulsion interface provided by SpaceX. The pusher interface, shown in Figure 19 will be attached to

a high powered wheeled vehicle that will fit into a receiver interface on the back on the pod. The maximum acceleration distance will be 800 ft.

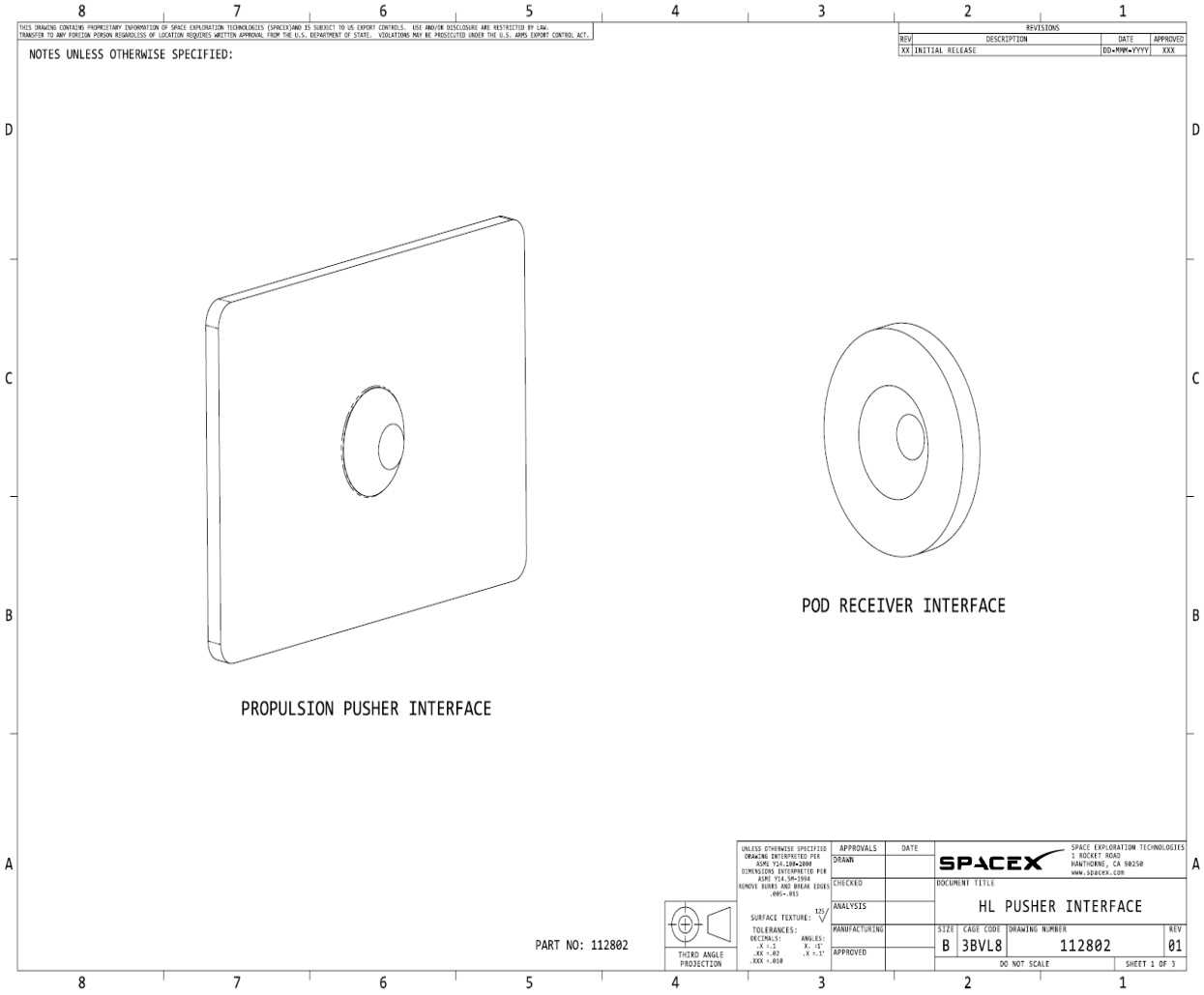

Figure 19. SpaceX Propulsion interface and pod receiver interface

The acceleration profile given by the propulsion interface is dependent on the mass of the pod. Figure 20 shows the acceleration profile of the HyperLynx pod.

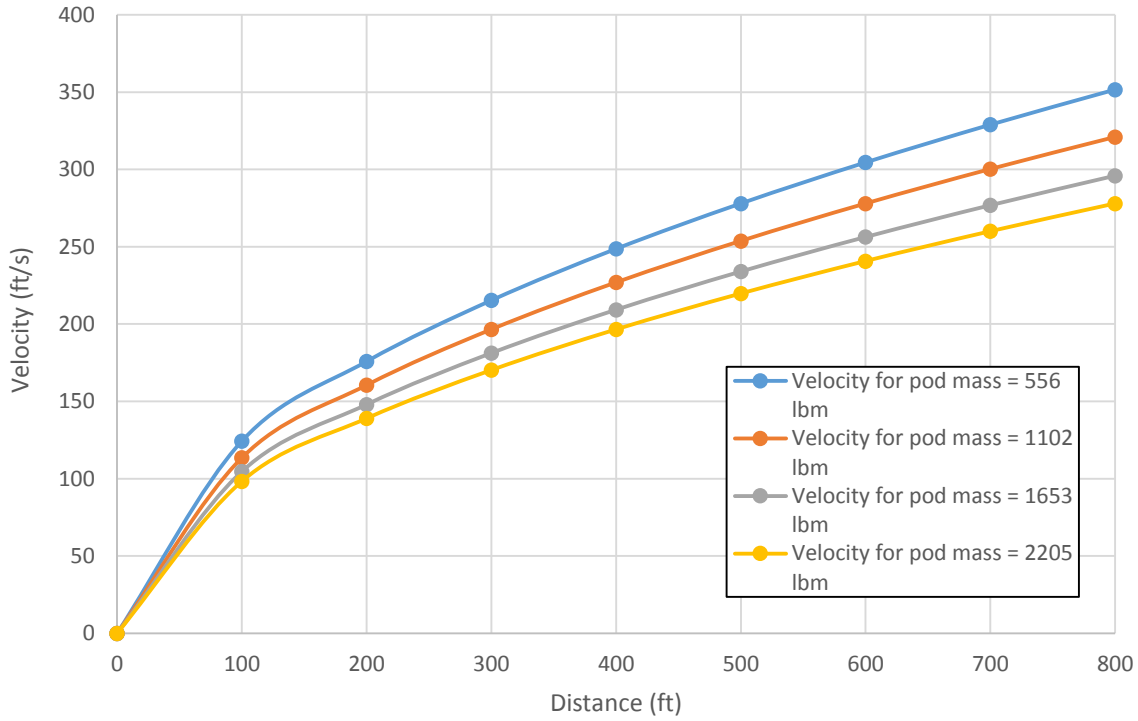

Figure 20. Pod Velocity during acceleration phase

The propulsion interface will be machined out of aluminum and welded to the frame. The interface to be attached to the pod is shown in Figure 21 and Figure 22 shows how the assembly fits together.

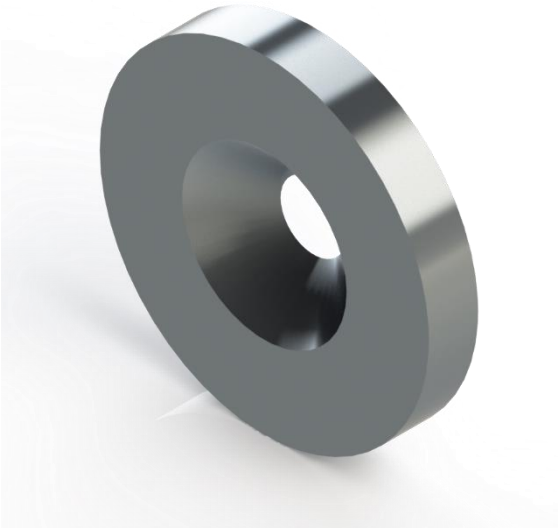

Figure 21. Pod Propulsion Interface

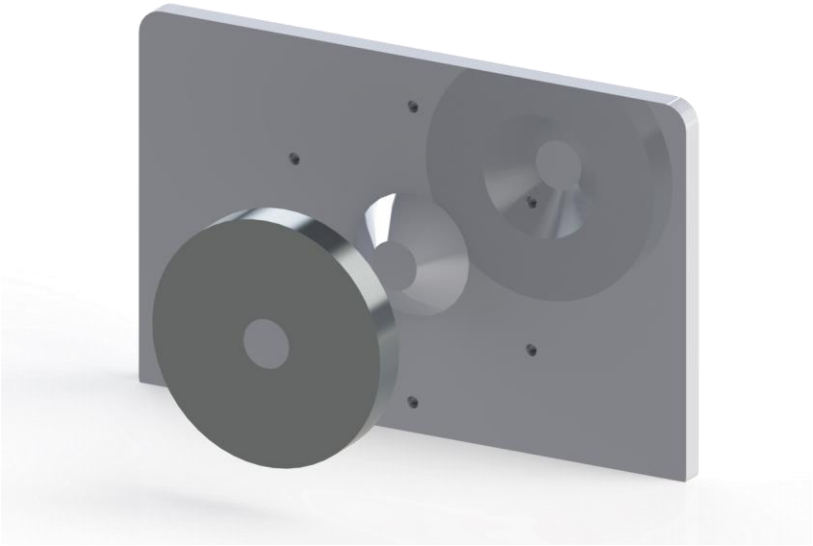

Figure 22. Pod Propulsion Assembly

8 LEVITATION

With a max acceleration distance of 800 ft from the SpaceX pusher interface the primary goal of the levitation subsystem is to decrease friction of any kind. At high speed, friction from bearings or wheels could cause increases in temperature that would cause failure due

to temperature as well as decrease efficiency of the pod and require additional propulsion throughout the test in order to maintain speed. In order to decrease the effect of friction, the pod will use magnetic field architecture designed by Arx Pax. This will allow the pod to levitate to heights of up to .79 in. and produce negligible friction.

The magnetic field architecture will work by generating a magnetic field which will induce electrical currents in the aluminum subtrack. These currents then create a secondary magnetic field which repels the original magnetic field (Arx Pax). The aluminum subtrack supplied by SpaceX in the mile long test track meets the criteria for this technology to be used as shown in Figure 23. It exceeds the recommended thickness during the first 200 ft, and exceeds the minimum thickness during the rest of the track. According to Arx Pax, at higher velocities the requirement for subtrack thickness decreases, therefore the subtrack is sufficient at all points along the test track as long as the pod remains in motion.

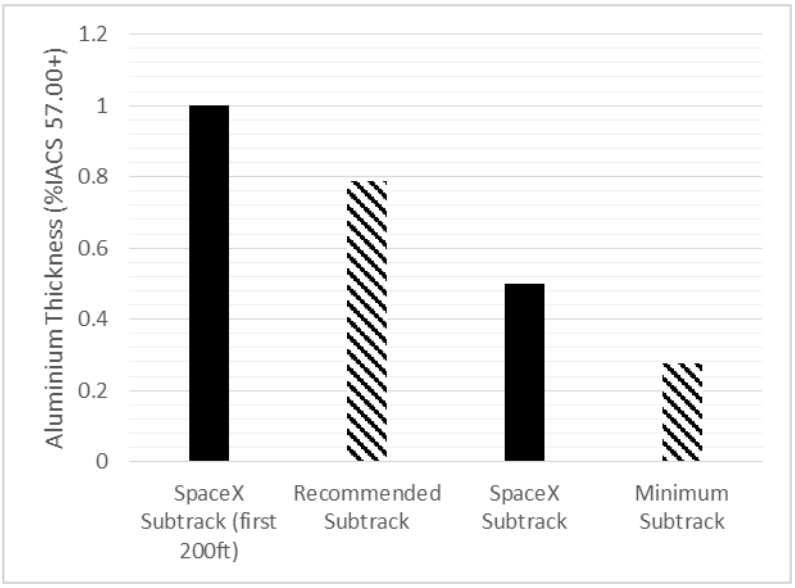

Figure 23. Subtrack Thickness Comparison

Arx Pax will supply HE3.0 engines shown in Figure 24 for use on the pod. The supplied Arx Pax Hover Engines have the flexibility to be mounted and controlled in many different configurations, allowing for different designs and different functionality.

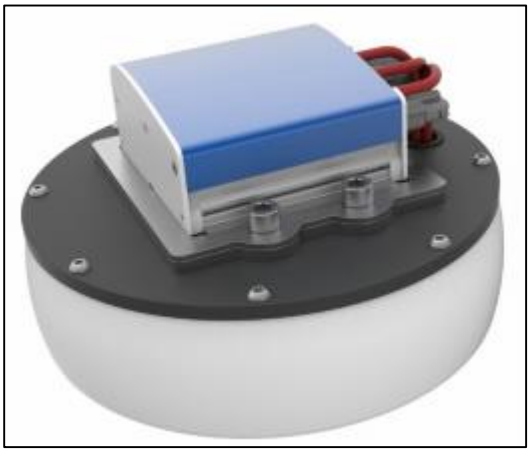

Figure 24. HE3.0 Hover Engine from Arx Pax

Actuating the hover engines allows the engines to contribute to pod braking, propulsion and lateral control by controlling the direction of its thrust. In order to actuate the hover engines, a separate actuating system has been designed to mount the engine and allow for control over its orientation. Figure 25. Effect of Actuationshows how the hover engine is actuated to provide additional propulsion, with a controlled rotation of the motor, B, and a tilt, A, the direction of propulsion will be C.

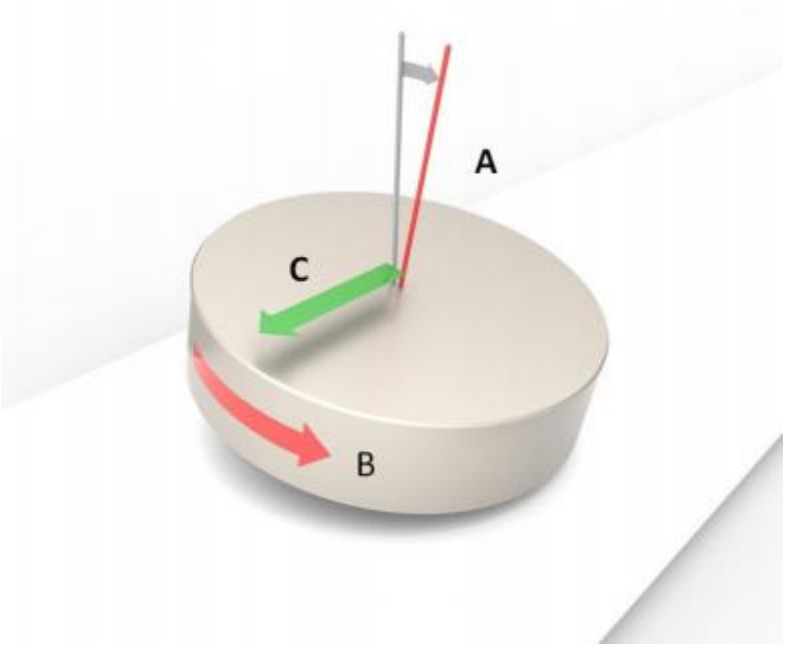

Figure 25. Effect of Actuation

The mounting and actuation bracket will be manufactured in two parts. Both pieces will be machined out of 1040 Aluminum and the top mount will be welded directly to the frame. The bottom piece will have holes drilled to attach the engine to the bracket. It will also be held within the top bracket, and actuated by a servo motor controlled through the pod CPU. This will allow control over propulsion and braking. The bottom mounting bracket is shown in Figure 26 and a thorough analysis was run at its maximum rated lift to ensure it would be structurally sound during operation. This FEA is shown in Figure 27.

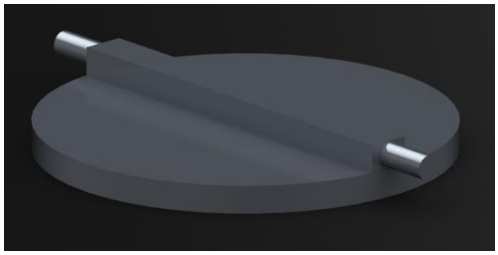

Figure 26. Mounting Bracket

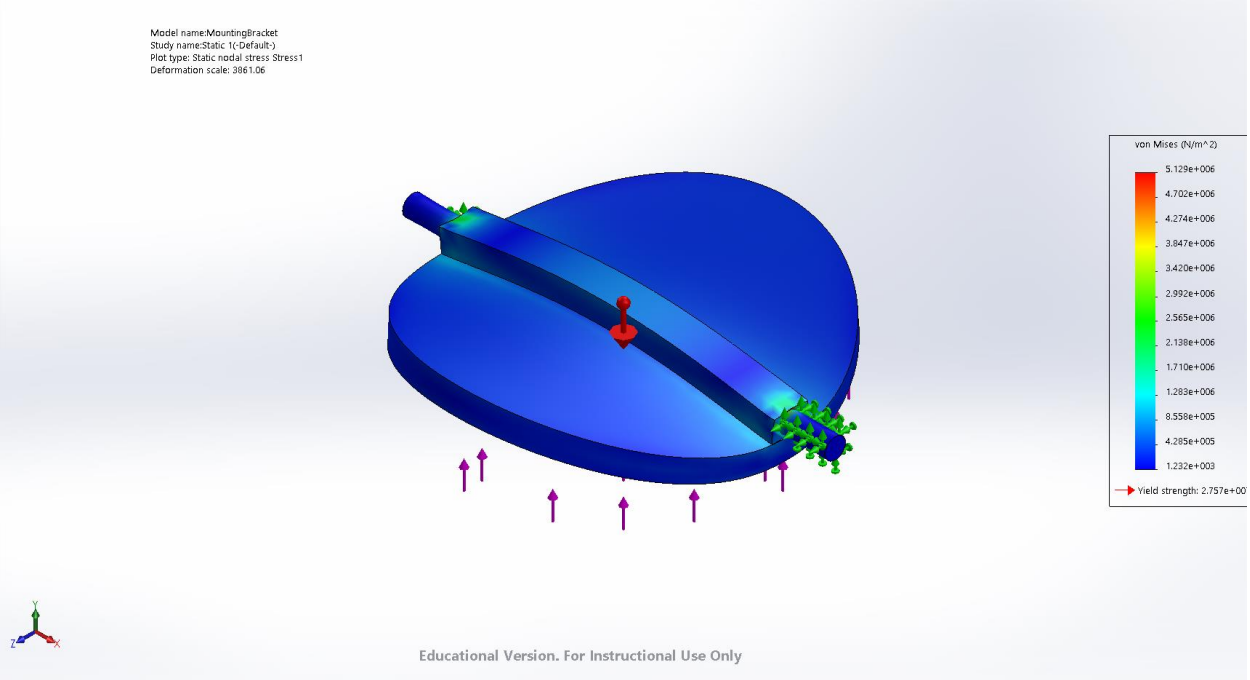

Figure 27. FEA of Bottom Mounting Bracket

The hover engines are still in the development stage. Arx Pax is continuing the development throughout the design and manufacture stage in order to maximize efficiency and payload capacity. The current design specifications shown in Table 3 are a minimum worst-case scenario and are expected to increase prior to delivery.

Table 3. HE3.0 Specifications

Rated Lift	55 kg
Hover Height	20mm – 5mm (varies based on payload)
Power Req. (Input Voltage 39V)	70 W/kg

In order to provide adequate lift, six Arx Pax motors will be installed on the pod at locations shown in Figure 28.

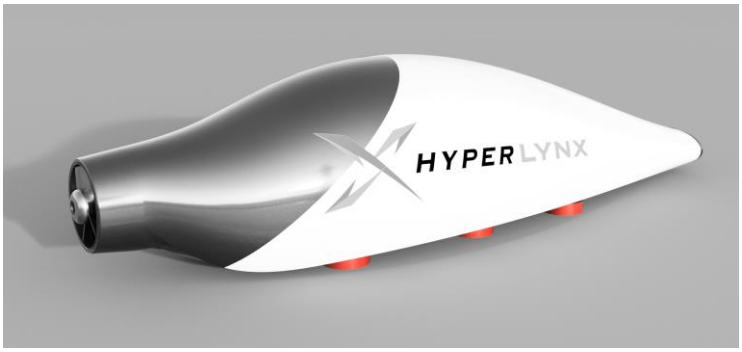

Figure 28. Placement of HE3.0

With each Arx Pax Engine costing $4,850, limiting the usage of these engines to only six is crucial to the feasibility of the pod's construction. At a cost of $29,100 the pod will be rated for a maximum lift of 364 lbs. Given the limiting factors of the levitation motors, this is the biggest design constrain.

Assuming a maximum payload, the hover engines will run at a .20 in. fly height, and require 11.55 kW of power while hovering. This will be supplied by the onboard battery system during motion, and the power umbilical supplied by SpaceX during the safety inspection and testing before motion begins.

9 POD POWER

Multiple factors for the pod operating systems have been assessed in order to design a viable power supply system. Onboard car batteries will be the primary source of power to the systems. The initial factor to be considered is the amount of power needed to run all the system components. Table 4 shows the calculated input power requirements for each system's components. These values are based on manufacturer specifications. Notably, the hover engines consume around 85% of the power drawn. This creates the first design constraint for the power system.

Table 4. Power Requirements for System Components

System Components	**Power Input Requirement [Watts]**
Intake Fan	1550
Hover Engines	11,550
Control System sensors	250
Actuators	192
Total	**13,542**

More important than the general power requirement for the components are the voltage and current specifications for each of the components running at nominal power settings. The standard power formula is used to analyze requirements. Each component has a specified operating voltage. This is the key factor is designing the power supply system. Table 5Table 5. Voltage and Current Requirements states the required voltage setting for the system components. The current is then computed to determine the power input values.

Table 5. Voltage and Current Requirements

System Components	**Voltage Req. [V]**	**Max Current Req. [A]**
Intake Fan	230 VAC	6.6 A
Hover Engines	39 VDC	150 A
Control System	5 VDC	1.5 A
Actuators	5 VDC	-

Table 5 also shows the maximum current requirements specified on some of the components. It can be noted that there is a wide range between the peak current allowed for the hover engines which is 150 amps and the 1.5 amps maximum current that can be fed into the control system. As the current power supply system will involve each system drawing power from the same power source a fuse block and regulators will be utilized to avoid overloading the circuits. The NewMar DST-20A Rackmount Distribution Panel will function as the main circuit breaker. It can accommodate up to a maximum of 80 VDC of distributed power. It features two circuits, A and B with ten inputs each rated at 450 amps. The A and B breakers can be connected in parallel offering a rating of 900 amps. Circuit breakers accompanying the panel can be chosen from a current rating of 5 amps to 100 amps. Figure 29 shows the circuit breaker panel.

Figure 29. Rackmount Distribution Panel Circuit Breaker

A voltage regulator will be used to generate a fixed output of 5 Volts for the control system components. An L7805CV voltage regulator by STMicroelectronics will be used to step down to 5 Volts, 1.5 amps for the control system. It is a linear regulator designed with thermal overload and short circuit protection within the design. It has a two percent output voltage tolerance.

Six 12 V car batteries can be connected in series to provide the required 72 V to the system. A high power, deep cycle battery designed for performance with multiple connected accessories was desired for this application. Optima Yellowtop lead acid batteries were chosen as they have high performance ratings. 81 amps is the highest current draw that can be experienced in the system due to the hover engines. To minimize weight, the Optima D51 Yellowtop Battery was chosen as it the lightest of the models and provides the maximum current requirement with the six batteries. The specifications for the battery are listed in Table 6. With an internal resistance of .0046 Ohms, the highest voltage loss calculated from Ohm's law would be .175 V from each battery. At only 1.5% of the input voltage, the loss is negligible.

Table 6. Optima D51 Yellowtop Battery Specifications for single battery

Voltage Output	12 VDC
Capacity rating	38 Ah
Internal resistance	0.0046 Ohms
Weight	26.0 lb
Dimensions	9.272 in. x 5.024 in. x 8.885 in.

The specifications for the Atmosphere V-16XL intake fan state an input voltage of 230 VAC. The hover engines, control system sensors, and actuators however utilize direct current voltage. An inverter will be used to convert direct current into alternating current to supply power to the intake fan. Two types of inverters were considered. One, a pure sine wave inverter (PSW) that transforms direct current into a smoothly varying alternating current

similar to a genuine sine wave. The other, a modified sine wave inverter (MSW) that produces a square wave that is an approximation of a sine wave. A comparison of the two is shown in Figure 30 referenced from the CivicSolar article.

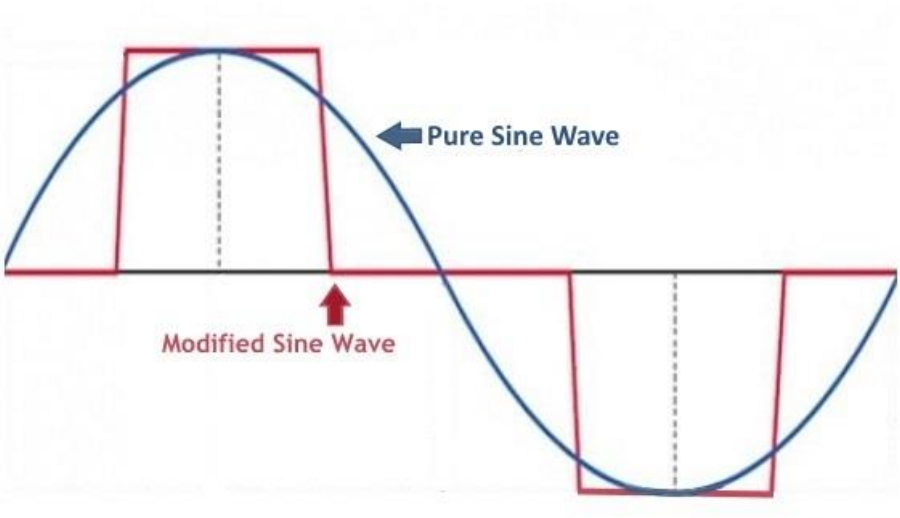

Figure 30. Sine Wave Comparison

A modified sine wave inverter provides more power in comparison as the area under the square wave is larger. However it has a higher probability to overheat due to this surge of power leading to damaged components. For this reason, a pure sine wave inverter will be used to convert DC power for the intake fan. The intake fan requires 230 VAC and 1550 Watts. A common guideline is to choose an inverter rated at least twenty five percent higher than the maximum power input on the appliance. The intake fan would need an inverter rated at 1938 Watts. The PROwatt SW 2000i power inverter by Xantrex Technology Inc. has all the necessary specifications. Table 7 shows the specifications on the PROwatt SW International inverter.

Table 7 . PROwatt Inverter Specifications

PROwatt SW 2000i

Continuous power	2000 W
Surge capacity	4000 W
DC input voltage	12 VDC
AC Output Voltage Range	230 Vac ± 10%
Weight	12.05 lb
Dimensions	4.5 in. x 9.5 in. x 16.5 in.

This model has a ninety percent efficiency which is acceptable. It has a safety factor of two with the surge capacity rated at a little over double the expected maximum input for the intake fan.

The power supply system will include the components previously discussed. Six 12 V batteries will be connected in series to provide 72 V. An inverter will convert direct current from the batteries to alternating current for the intake fan. The circuit breaker will act as a fuse box for the control system circuit to ensure the system is not overloaded with high current. A regulator will also step down the voltage for the control system accessories and sensors. Figure 31 shows a block diagram of the power distribution for the different systems in the pod.

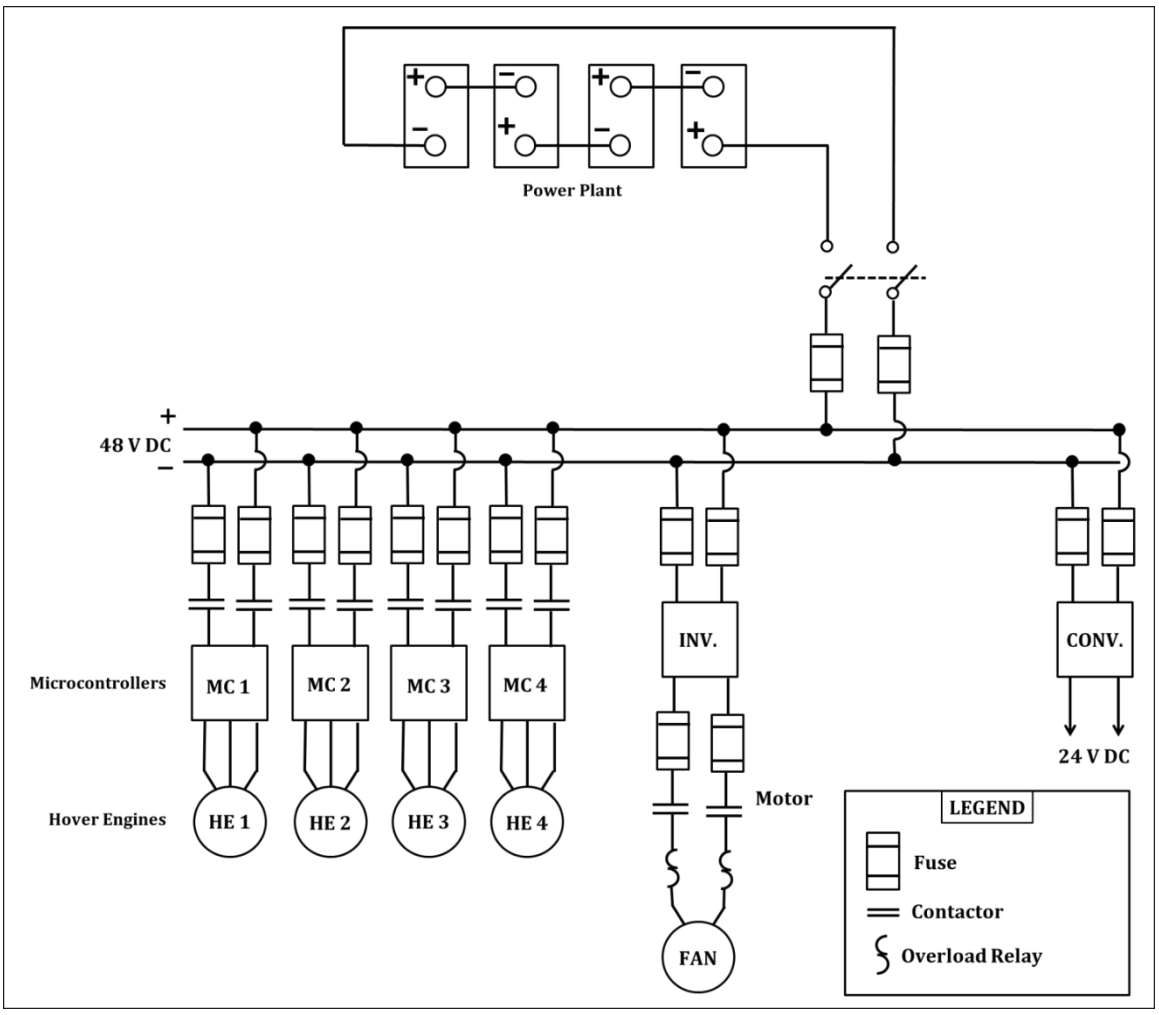

Figure 31. Hyperlynx Power Distribution Diagram

10 CONTROL SYSTEM

The controls system will command, regulate, and record the various functions throughout the pod. Broadly, the pod control system is a network of sensors, actuators, and logic controllers that dynamically alter system outputs. Custom software code will be developed to execute system commands based on sensor input data. The core processing and communication hub will be powered by a 24 VDC input signal converted from a 72 VDC main battery source. Power input will be conditioned and distributed at circuit voltages through a National Instruments PS-16 10 Amp power supply. This power supply unit is modular, and will interface to a NI cRIO 9112 8-slot chassis. The PS-16 power supply was selected because it is optimized for a wide range of temperatures, high vibration/shock, heavy accessory loads, and battery-based power inputs. A NI-cRIO 9025 controller will execute pod commands. This controller is optimized for extreme environments and battery power, and can run on voltages as low as 6 V. The processor features 512MB DDR2 RAM, giving the controller enough processing power to manage complex system inputs with microsecond response. The next module on the control chassis is a NI Moxa EDS-205A-T Ethernet switch. This switch will be tethered to the system controller via hardwired RS-232 serial ports. The switch will ultimately interface to a SpaceX-provided network access panel to enable wireless communication in the test track. Wireless communications will facilitate off-board data acquisition, and provides an avenue for remote control (for example, emergency stop). Finally, sensor and actuators will connect to a NI 9381 multifunctional I/O module. The module features thirty-two differential analog I/O ports that can be configured for digital communication when necessary – a setup compatible

with current pod I/O needs. The system chassis, controller, and I/O module are shown in Figure 32 below.

Figure 32. System Control Chassis, controller, and I/O Module

Not shown in Figure 32 are the system power supply module and Ethernet switch. The Ethernet module will occupy one of the free slots from the figure, and the power supply unit will use the remaining two chassis slots.

Sensor input data will consist of position, velocity, acceleration, attitude, pressure, temperature and power consumption. This data will be processed continuously during transport. Table 8 lists the measurement, expected frequency range, signal conditioning, supplier, and price for each sensor.

Table 8. Sensor Information

Measurement	Sensor	Frequency Range	Signal Conditioning	Supplier	Price
Vibration	Accelerometer	<50 kHz	18-30 VDC Current Regulating Diode	PCB Piezotronics	$310.00
Speed	Proximity Probe	<25 kHz	10-30 VDC 15mA plus load	SPI Sensor	$50.00
Temperature	RTD Thermocouple	<10Hz	Noise rejection, excitation,	National Instruments	$104.00

			cold-junction compensation		
Pressure	Dynamic Pressure	<170 kHz	18-30 VDC	Omega	$300.00
Stability	Gyroscope	<25 kHz	4.5-16 VDC	Discrete Semiconductor	$50.00
Location	Photoelectric	<100 kHz	30 VDC	Micro Epsilon	$400.00
Current/Voltage	Energy	<160 Hz	30 VDC	Vernier	$69.00

Spacex will also provide a Mide Slam Stick X Aluminum logger in order to collect and log environmental data experienced in flight. The slam stick logger will be mounted to the chassis of the pod and will remain parallel to the plane of motion within 5 degrees at all times. The logger will be installed at the test track ingress staging area, and uninstalled in the egress exit area after the competition test run. Data will then be extracted and reviewed.

All sensors and final control elements communicate with the NI controller via differential I/O ports. Table 9 shows the current input/output list for the pod.

Table 9. HyperLynx Pod I/O List

Digital Output (DO)	
Contactor 1	On Command
C2	""
C3	""
C4	""
Hover Engine 1	On Command (DI 1)
	Tilt Command (DI 2)
HE2	""
	""
HE3	""
	""
HE4	""

	""
Brake Release	On Command
E-Stop Relay	On Command
Digital Input (DI)	
Contactor 1	On Status
C2	""
C3	""
C4	""
Motor	On Status
Photoeye	On Status
E-Stop Relay	On Status

Analog Output (AO)	
HE1	Brake (AI 1)
	Throttle (AI 2)
HE2	""
	""
HE3	""
	""
HE4	""
	""
Accelerations (XYZ)	(DAQ/Estop)
Brake Pressure Setpoint	

Analog Input (AI)	
Battery Voltage	
Brake System Pressure	
Accelerometer	(XYZ)

All inputs and outputs from Table 9 will be processed using NI LabVIEW or Linux-based software running on the pod controller module.

Spacex will provide a network access panel (NAP) in order to connect the control system to the wireless communications network. An Ethernet 15 port switch will be at the ingress and egress staging and used for Wi-Fi connection. The network access panel will require 20 W of power, and will be located at the pods rear. The panel will face perpendicular to the track and have a clearance of 0.25 inches. The modular Ethernet switch inside the pod will

hardwire to the NAP panel using RJ45 Ethernet sockets common to both devices. Figure 33. Network Access Panel Rendering shows a rendering of the network access panel.

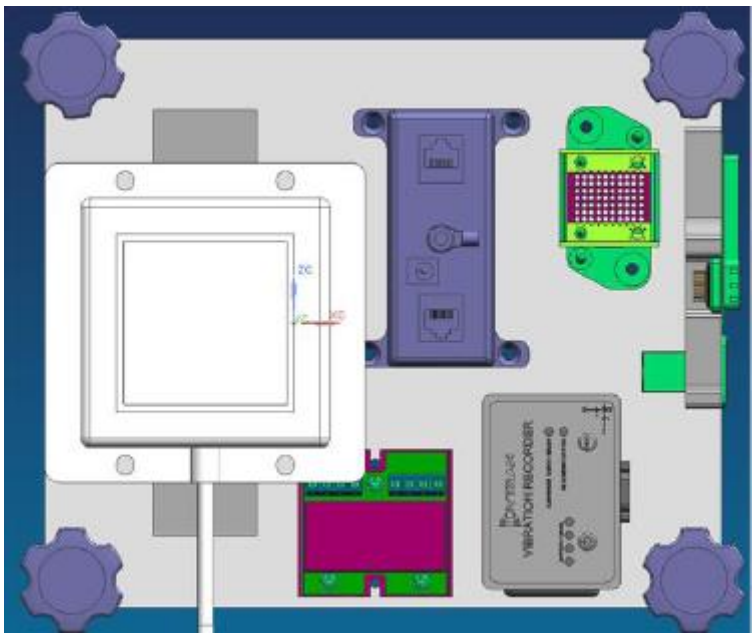

Figure 33. Network Access Panel Rendering

The largest accessory loads on the pod logic control system are the four DC motor controllers mounted to the ArxPax hover engines. Each controller utilizes two analog I/O ports each that interface to the master NI 9381 I/O module. These analog communication channels create feedback control systems unique to each motor. Ultimately these systems dictate the amount of power each motor receives. Controlled power distribution to the motors will balance the pod for neutral levitation, tilt the pod four degrees forward for supplemental thrust, or tilt the pod four degrees back for supplemental braking. Each of the hover engines purchased through Arx Pax interface to Accelerated Systems Cadmium Series BAC 200072100 motor controllers mounted on top of the hover engines. These controllers monitor and control throttle to the DC brushless motors that actuate the hover engines to a desired orientation. Figure 34 displays a rendering of the motor controller.

Figure 34. Rendering of Hover Engine Motor Controller

To process data-intensive applications while maintaining micro/nanosecond response time - and to guarantee pod safety - a robust control system, one that remains reliable under high temperatures and vibrations, is necessary for a medium-scale pod. The control system described above was selected for these reasons. Each hardware component interfacing to the control chassis, including the chassis itself, is rated to 50g's of shock and can operate in temperatures ranging from below freezing up to 170^{o}F. Since the pod will operate near vacuum conditions, the temperature ratings of all system electronics are required to perform when high operating temperatures occur. Given the speed and acceleration profiles of the pod, the system was chosen for physical reliability in a potentially punishing vibration environment. The pod is designed for dynamic stability at high speeds. However, the pod will also be designed to safely execute a system stop even if extreme instability occurs. Furthermore, since the pod power plant is battery-based, reserve power must be available in the control power supply to execute a system stop if the main batteries lose power. Cheaper systems, for example, a system using a Raspberry Pi controller with integrated I/O ports, have been evaluated. These options are suitable for miniature scale

pod application, but lack the memory, processing power, environmental reliability, and overall toughness required for the safe launch of a 1000-lb pod.

11 BRAKING

The pod will be expected to reach a maximum speed of 240 mph. To reach this maximum velocity the pod will be pushed the distance of 800 ft by the SpaceX provided propulsion interface.

In order to stop this pod in a controlled manner and at safe distance, calculating the amount of braking force and proportioning the brake loads is essential. As the velocity of the pod increases the braking forces needed also increase. Using the maximum velocity of 240 mph, the braking forces were calculated with varying decelerations. Also the amount of braking force was calculated based on the pod's center of gravity and placement of brakes in front of the center of gravity of the pod as well as behind. Figure 40 displays the free body diagram that was used to calculate the braking forces.

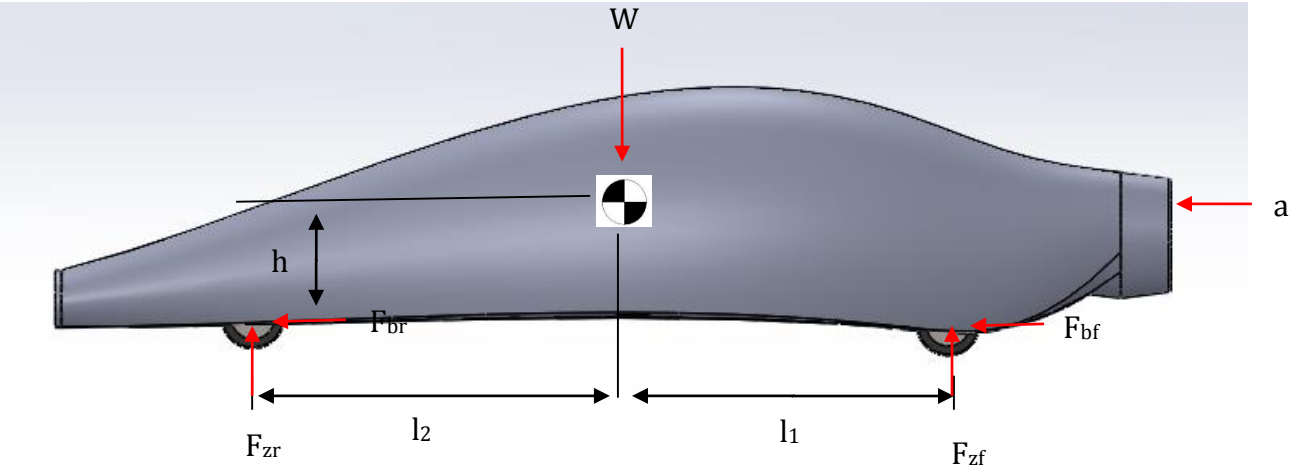

Figure 35: Freebody Diagram of Braking

Brake proportioning is designed to maintain control of the pod. The following equations were used to compute the amount of braking force needed due to the rate of deceleration.

$$F_{zf} = W\left[\frac{l_2}{L} + \frac{h}{L}\left(\frac{a}{g}\right)\right] \quad \textit{Equation 5}$$

$$F_{zr} = W\left[\frac{l_1}{L} - \frac{h}{L}\left(\frac{a}{g}\right)\right] \quad \textit{Equation 6}$$

$$F_{bf} = \mu F_{zf} \quad \textit{Equation 7}$$

$$F_{br} = \mu F_{zr} \quad \textit{Equation 8}$$

$$K_f = \frac{F_{bf}}{F_{bf}+F_{br}} * 100 \quad \textit{Equation 9}$$

$$K_r = 100 - K_f \quad \textit{Equation 10}$$

F_{zf}: upward force on front tires, F_{zr}: upward force on rear tires, W: weight of pod, l_1: center of gravity distance behind the front axle (5.05 ft), l_2: center of gravity distance ahead of rear axle (4.95 ft), L: wheelbase of pod (10 ft), h: center of gravity distance above the ground (0.92 ft), a: acceleration, g: gravity, μ: coefficient of friction, F_{bf}: front braking force, F_{br}: rear braking force, K_f: percentage of braking force applied to front brakes, K_r: percentage of braking force applied to rear brakes.

In order to stop the pod with equal braking force between the front and rear, the deceleration of the pod would need to be around 0.11g's. Due to the velocity of the pod that would not be a realistic deceleration rate therefore brake proportioning is necessary for pod stability. Looking at Figure 36, as the deceleration rate increases the braking force on the front brakes increases. At the same time the rear braking force decreases. In order to stop the pod at 1g of deceleration it would take approximately 415lbf (60%) of the

braking force to be applied to the front brakes and 290 lbf (40%) applied to the rear brakes.

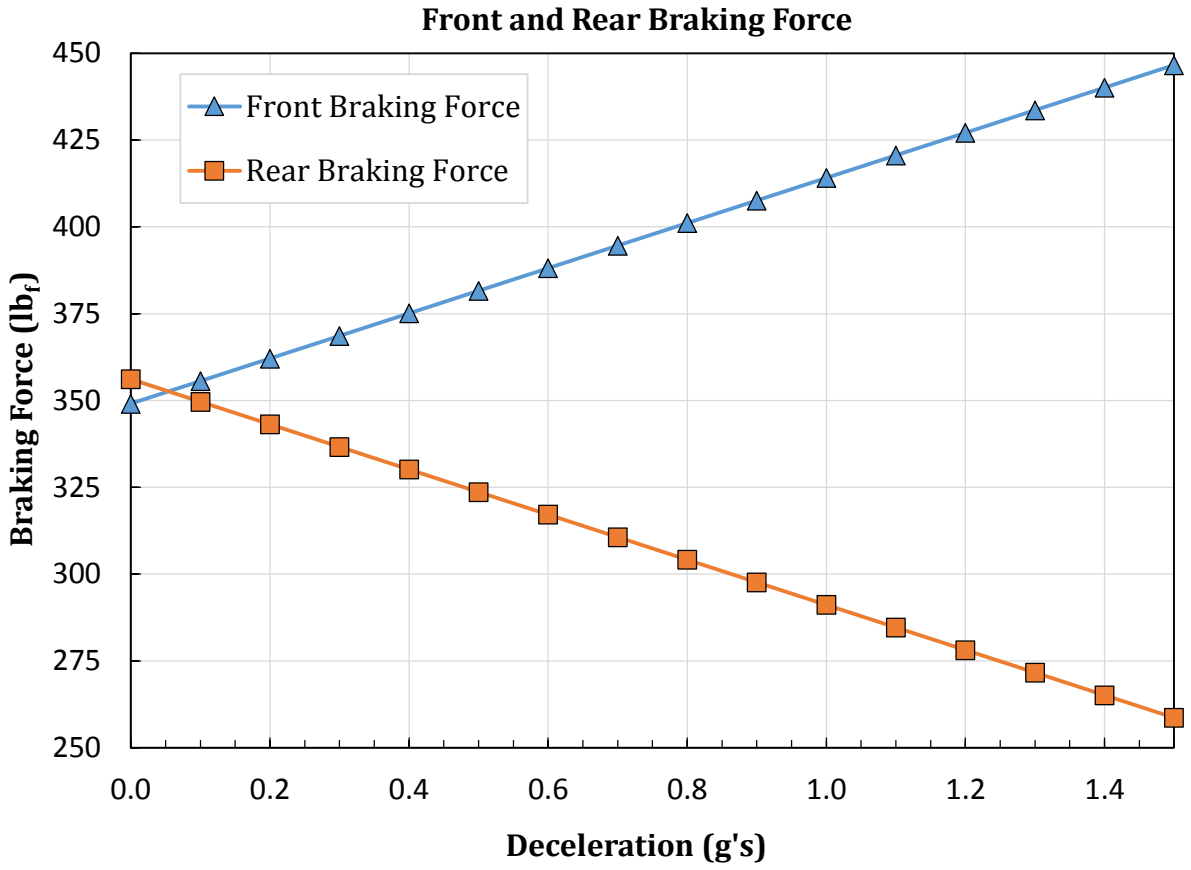

Figure 36: Force Applied to Front and Rear Brakes

Another important consideration included in the braking design is the rate of deceleration due to the time and distance needed for the pod to completely stop. The following equations were used to calculate the time, *t*, and distance, x_b, it takes to come to a complete stop.

$$t = \frac{(v_f - v_i)}{a} \qquad \textit{Equation 11}$$

$$x_b = \frac{(v_f^2 - v_i^2)}{2a} \qquad \textit{Equation 12}$$

At the maximum velocity of 240 mph and a rate of deceleration of 1g the pod will brake for 11 seconds for a braking distance of 1921 ft.

The braking system will use multiple deceleration mechanisms. The initial braking mechanism will utilize the Arx Pax levitation engines. At the rated hover height between .2 in. and .79 in., which is dependent on the total payload of the pod, the Arx Pax will be able to tilt between 1 to 4 degrees. Utilizing this ability to tilt, the Arx Pax will be designed not only levitate the pod but will also create a resisting force for braking when angled in the proper direction. Figure 37 displays the Arx Pax tilt angle. The amount of braking force that the Arx Pax will be able to supply will be determined from the tilt angle once complete specification on the Arx Pax is provided. The mounting of the Arx Pax engine is designed to only allow tilting of the engine in a forward and backward tilting motion. Also by limiting the Arx Pax ability to tilt, the stability of the pod can be better controlled during braking where possible varying movement of the Arx Pax engine would not be desirable.

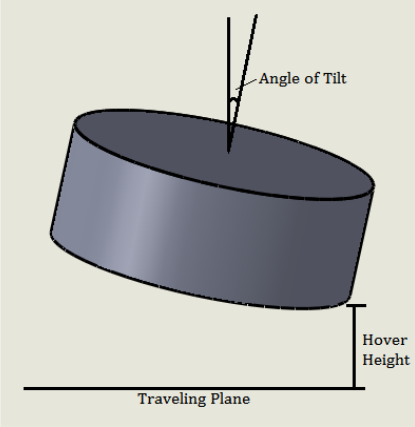

Figure 37: Arx Pax Tilt Angle

The primary braking system will be a landing gear assembly where all the tires will be of equal size and attached symmetrically on the pod. Figure 38 displays the landing gear.

The tires will be 10 inches in diameter and will be a width of 6 inches. The size of the tire was chosen in order to brake on the concrete pad verse the aluminum plate. This will give the tire to dry concrete surface a 0.82 friction of coefficient.

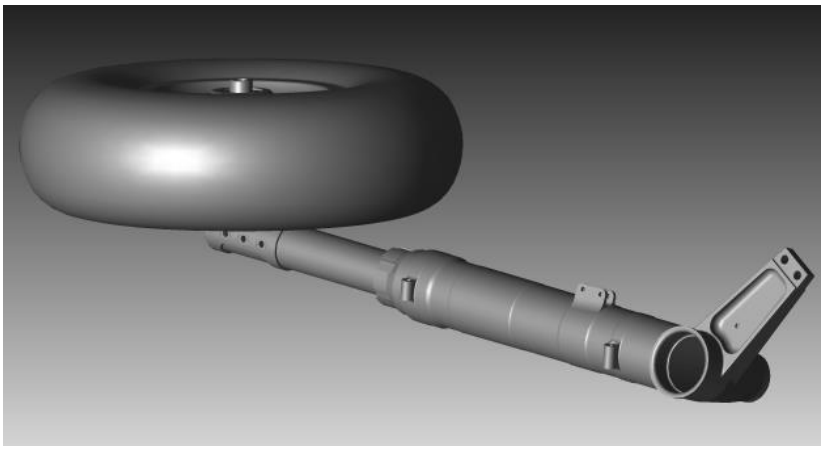

Figure 38. Landing Gear

Four wheels will deploy and the Arx Pax engines will no longer provide levitation but will instead be used in the aide of slowing down the pod. Then, an internal caliper brake system will be initiated on the rail to aide in slowing down the high speed pod. As seen in Figure 39, the way the regenerative braking system is applied is by reversing the electric motor causing it to run backwards which will slow down the wheels. The electric motor will act as a generator providing energy back to the battery {from prelim}.

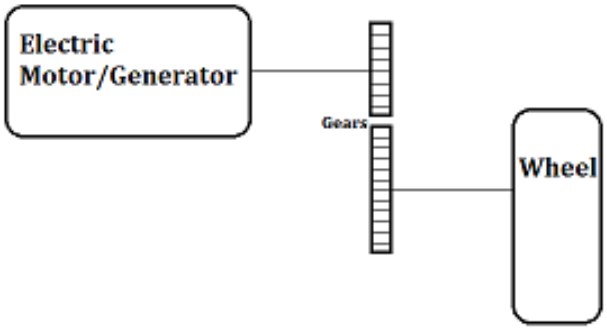

Figure 39: Simple Design on Regenerative Braking System

Once the two initial braking mechanisms have been initiated, disc brakes will be applied using an electric linear actuator. The brake pads will be made of ceramic which has a .15 coefficient of friction. Ceramic brake pads are able to withstand high temperatures and cause less wear on the brake rotors due to the material make up of ceramic pads. Ceramic material is known to withstand temperatures ranging from 1832°F to 2912 °F. Figure 40 displays the temperatures that the braking system will endure for stopping at different velocities therefore the ceramic brake pads should not see temperatures higher than 390°F according to the calculations. The braking temperatures are calculated using the following equations where *KE* is the kinetic energy, *m* is the mass of the pod, v_i is the initial velocity, v_f is the final velocity, *S* is the specific heat, and ΔT is the temperature rise at the brakes.

$$\mathrm{KE} = \frac{1}{2}\mathrm{m}\left(\mathrm{v_i^2} - \mathrm{v_f^2}\right) \qquad \textit{Equation 13}$$

$$\Delta T = \frac{KE}{Sm} \qquad \textit{Equation 14}$$

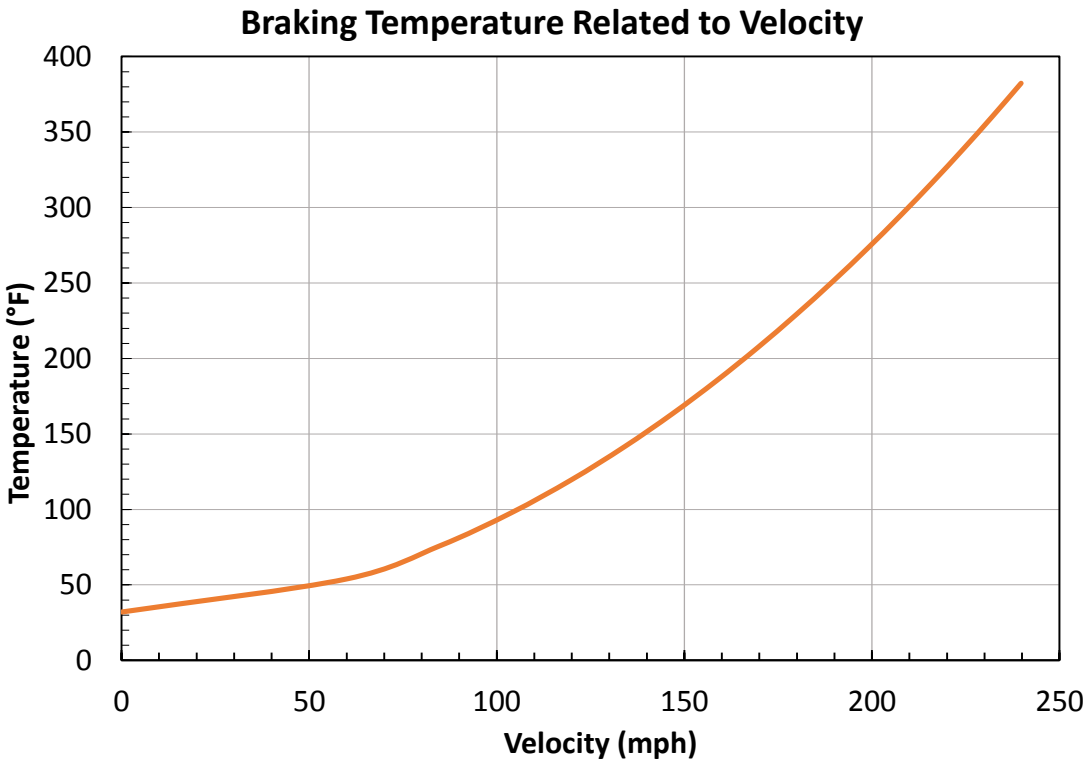

Figure 40: Braking Temperature

Table 10 shows the components needed for this braking.

Table 10. Component List

Component	Company/Model Number	Weight	Cost
Landing Gear	Grove Aircraft (RV-8 Airfoil Lightweight Gear)	15 lb per gear	$2000 per landing gear
Wheel & Brakes	Grove Aircraft (58-238)	7.33 per wheel and brake kit	$1200 per pair
Brake Pad	Grove Aircraft (066-105)	0.75 lb per pad	$36.50 for 4 pads
Linear Actuator	Electrak 10	12.7 lbs	TBA
Tire	Aero Trainer (5x5)	4.4 lbs	TBA
Total		**110 lbs**	

12 WIND TUNNEL TESTING

Wind Tunnel Testing Set Up

To simulate the conditions that the pod may experience, wind tunnel tests needed to be performed on a scaled down version of the Hyperloop pod and test track. The model track is a 3 in. inner diameter PVC tube. The model track is scaled to 23.5:1 reduction in the size of the full scale model. Figure 41 shows the 3 in. PVC tube with an aluminum rail down the center.

Figure 41. Test Tube and Rail Assembly

The model of the pod was 3D printed using an Objet printer. Figure 42 is the 3D printed model after wind tunnel testing, and Figure 43 is the model that was used to create the 3D printed model .

Figure 42. 3D Model (Cracks happened after testing)

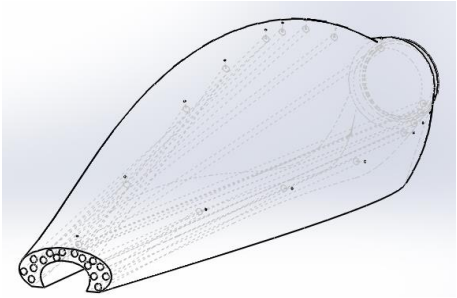

Figure 43. Model for 3D Printer

The test model has 1/16 in. holes placed along the top and side of the model. The pressure tap holes are placed to measure the transition of the pressure across the body. The pressure tap holes were fed into a channel that is a 1/8 in. diameter and those channels are routed through the pod to the back. Figure 44 is a picture off the 1/16 in. tap holes that are on the surface

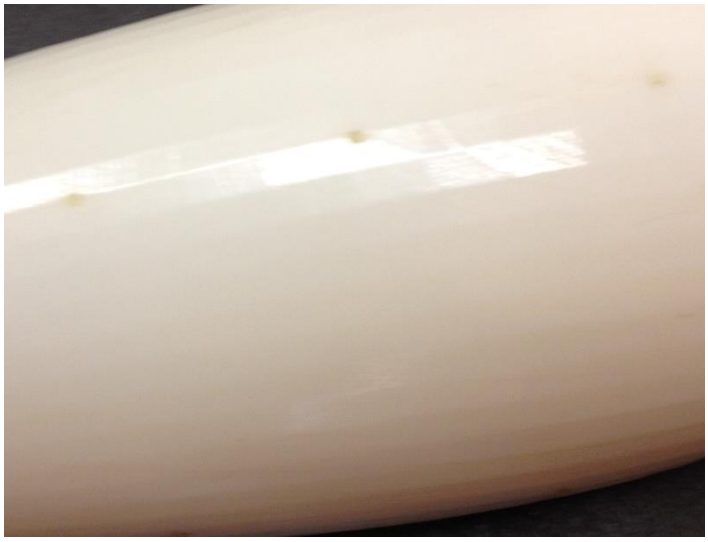

Figure 44. 1/16in. Pressure Tap Holes

The 1/8 in. holes were connected with 1/16 in. inner diameter brass tubing that used to connect with the Tygon tubing on the pressure transducer as shown in Figure 45.

Figure 45. 1/16 in. tubing connected to 1/8 in. channels

To interface the tube and the model to the wind tunnel, a mounting fixture was created. The fixture allowed the tube to be suspended in the wind tunnel. Velcro strips were placed on the tube and the model to keep the model secure in the tube. Tygon tubing connected the pressure transducer to the brass tubing at the end of the model. Figure 46 shows the 3D model of the mounting assembly of the tube and model interfaced with the wind tunnel. Figure 47 shows the constructed rig. Figure 48 is a front view of the mount assembly in the wind tunnel.

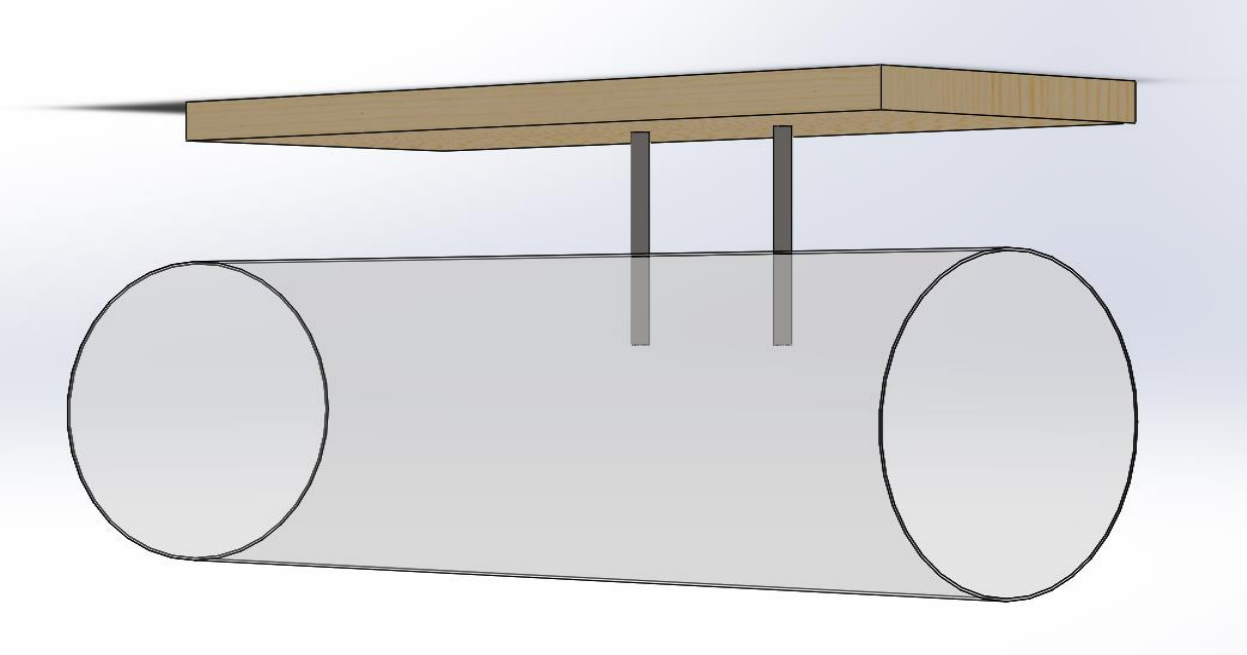

Figure 46. 3D Model of Wind Tunnel Fixture

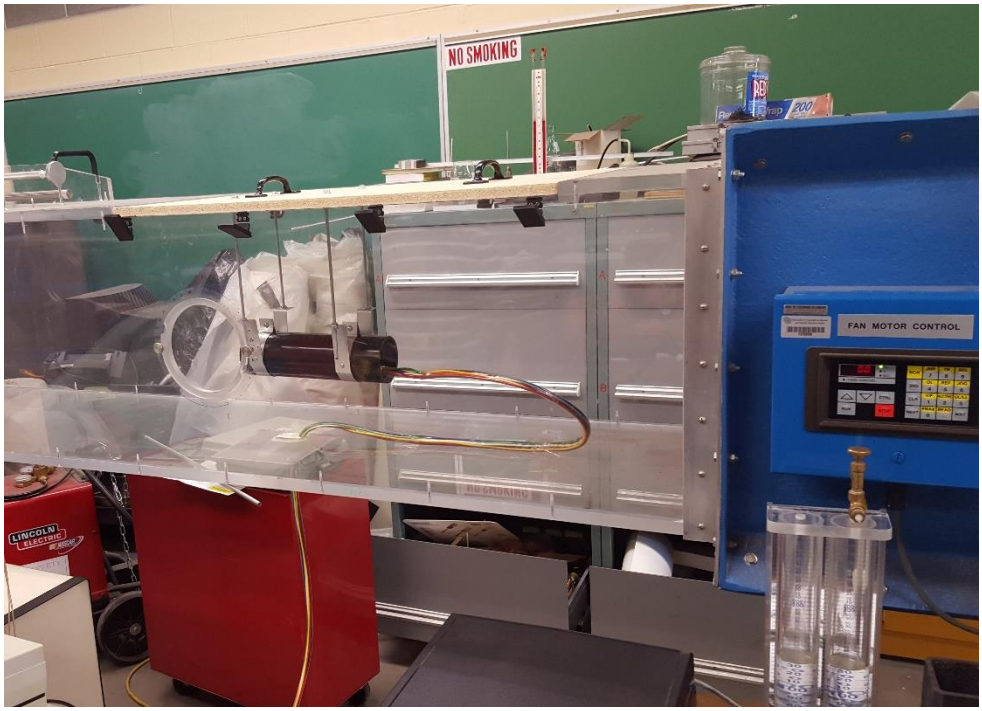

Figure 47. Wind Tunnel Mount

Figure 48. Front View of Mount Assembly in Wind Tunnel

A pitot-static tube was used to determine the speed of the air flowing in the wind tunnel. The tube was connected to a pressure transducer to measure the free-stream dynamic pressure, *q*. The pod had 14 holes tapped at specific locations and the difference between the local pressure at each tap location and the absolute pressure of air in the wind tunnel were recorded using the pressure transducer. The speed, *V,* of the air in the wind tunnel was computed from the dynamic pressure using

$$V = \sqrt{\frac{2q}{\rho}} \qquad \textit{Equation 15}$$

where ρ was the density of the air in the wind tunnel. The density of the air in the wind tunnel was computed using the ideal gas equation of state. The results for the experiment are shown in Table 11.

Table 11. Surface pressures at each tap

Tap #	Pressure (Pa)
1	82141
2	82136
3	82121
4	82148
5	82142
6	82138
7	82171
8	82145
9	82174
10	82164
11	82134
12	82137
13	82133
14	82128

In order to validate the experiment data, flow simulations were run on the model. Figure 49 shows the flow trajectories around the pod with air traveling in the negative z direction. The simulations were run assuming a free-stream velocity of 101 mph and environment pressure of 82,163 Pa, the same conditions as the wind tunnel experiment.

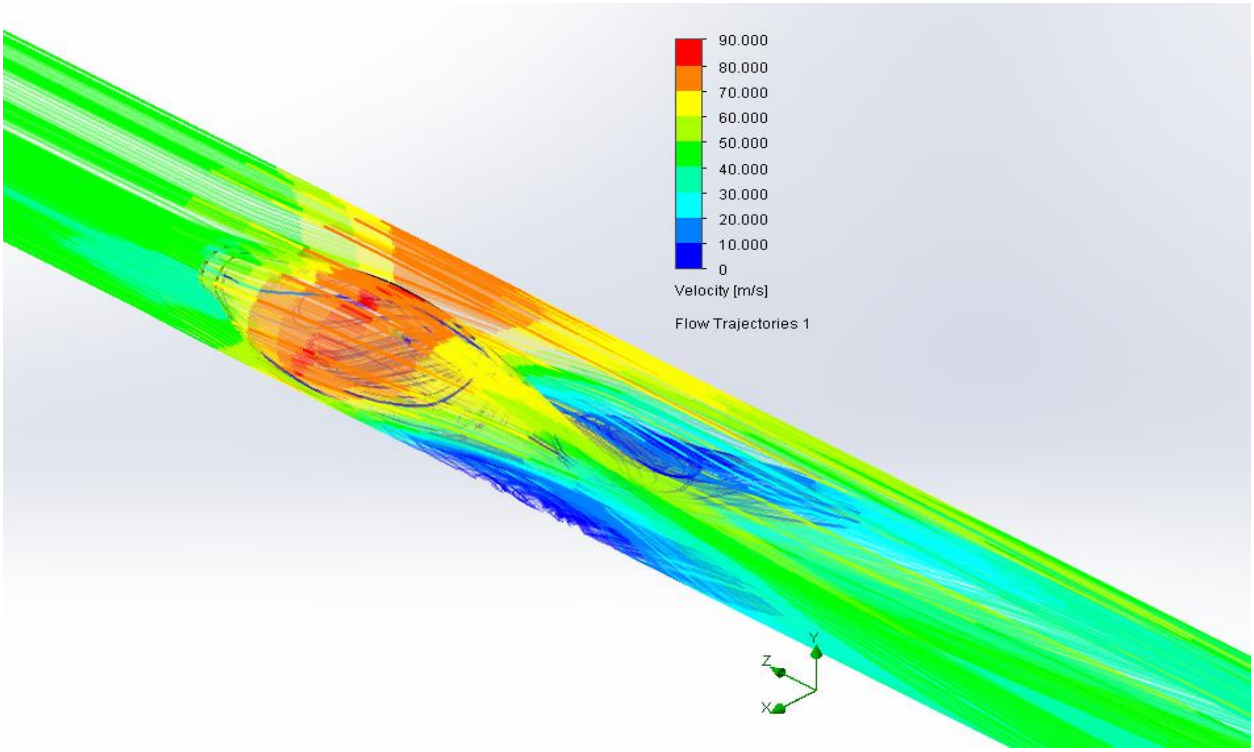

Figure 49. Velocity flow trajectories around the pod

Figure 50 shows where the taps are located and the pressure contours based on the computational fluid dynamics simulation results.

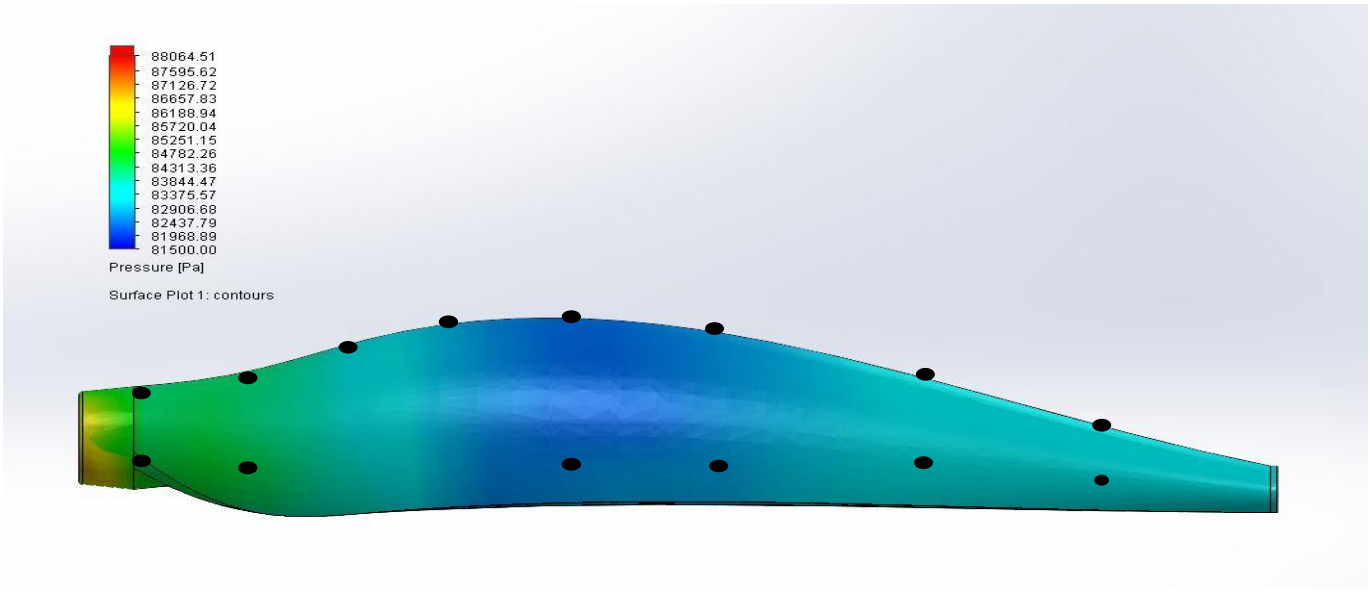

Figure 50. Side view of the model pod showing pressure tap locations and pressure contours

The experimental data shows that at any given tap, the surface pressure is between 82,100 Pa and 82,200 Pa. The simulation shows that the pressure is highest at the front taps, around 84,000 Pa, and decreases as the pod cross-sectional area reaches a maximum. At this area, the pressure is near 82,000 Pa. Then, the pressure increases slightly and remains uniform towards the back of the pod at around 83,000 Pa. Figure 51 and Figure 52 show additional images of the testing environment and process.

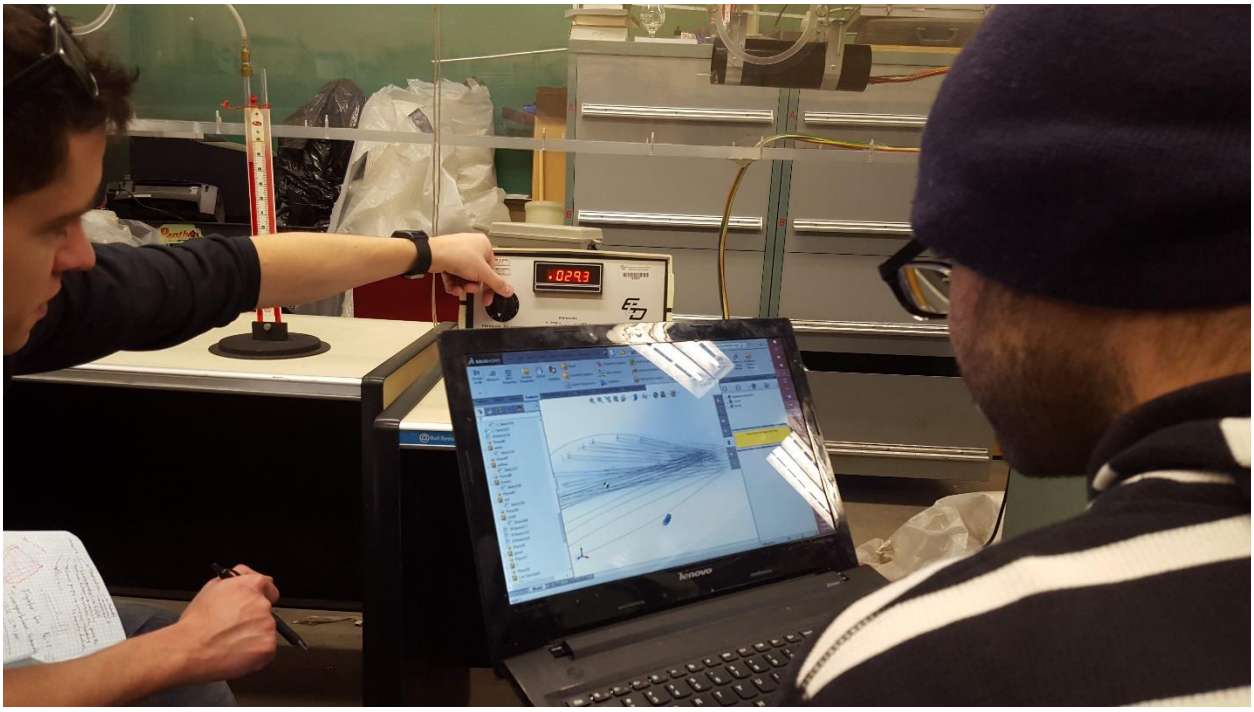

Figure 51. Wind Tunnel Testing

Figure 52. Wind Tunnel Testing Part 2

13 POD WEIGHT

The Hyperloop concept relies on the pods inside the tube traveling at speeds near Mach 1, or around 700 miles per hour. Although the prototype pod will not be able to go that fast, one way to achieve high speeds in the competition is to optimize the weight of the pod. Currently, analysis is being performed in each subsystem category to optimize the weight. This analysis entails structurally analyzing the frame and body though finite element analysis to minimize the weight without compromising strength. As well, various construction techniques are being analyzed to determine the lightest material possible for each component. Individual weight optimization is detailed in each subsystem of this report. Table 12 shows the weight estimate for the pod.

Table 12. Pod Weight Estimate

Component	Estimated Weight

Frame	376
Body	312
Intake Fan	66
Batteries	44
Brakes	50
Landing Gear	39
Control System	11
Levitation	90
SpaceX Add-ons	162
Total	1150

14 BUDGET

Table 13 is a detailed budget for the manufacturing of the pod.

Table 13. Estimated Budget

Subsystem/Component	**Price**
Frame (Carbon Fiber ABS & Aluminum)	$3,000
Body (Carbon fiber)	$1,400
Fan and Ducting	$1,027
Battery	$500
Brakes	$500
Landing Gear Assembly	$500
Controls	$4,104
Levitation (Arx Pax™ Engines)	$30,000
Miscellaneous	$500
Total Estimated Budget	$41,531

15 MEDIA OUTREACH & FUNDRAISING

Throughout the course of the project, fundraising has been a huge focus of Team HyperLynx. The team has actively sought media coverage and community involvement in order to raise funds for the project. In addition to the $2,400 provided by the school, a successful Kickstarter raised $6,658 with 88 backers, averaging $76 per backer.

In addition to the Kickstarter, Team Hyperlynx received publicity from several news groups, blogs, radio stations, and companies including ABC News, CBS News, Colorado Public Radio, Inverse, and the Colorado Department of Transportation. Team Hyperlynx also attended the Colorado Department of Transportation, Transportation Matters Summit and met with the Executive director of Transportation as well as some leading engineers and business men and women in the transportation field. Team HyperLynx attended the Future of Transportation Summit, hosted by the University of Colorado Denver.

For upcoming events, competitions and fundraising events, a display has been built that will help those who are unfamiliar with the idea of the Hyperloop visualize the project.

Figure 53. Visual Aid for Events

This visual aid should help raise more money for the project.

For future funding, Team Hyperlynx intends to seek the remaining money from sponsors of the SpaceX design weekend in January 2016. Furthermore, the team will follow up with

companies that have been contacted throughout this semester after a new fiscal year starts and there their funds are more freely available.

Team Hyerlynx has an active twitter, Facebook and independent website which can be found at denverhyperlynx.com.

16 CONCLUSION [INCOMPLETE]

17 RECCOMENDATIONS/PATH FORWARD

After much analysis, it has been determined that in order to be competitive in the competition, the weight of the pod must be decreased. Over the next couple weeks, a new frame design will be analyzed. It will take the 14ft long pod and reduce its size to 6ft, this will decrease the weight substantially and allow for increased acceleration. In addition, at low speeds, the fan/compressor makes a marginal difference, and for the power that it draws and weight that it adds to the pod it has been deemed unnecessary. For scaling up, and for higher speeds over longer distances the fan/compressor would make a bigger difference as the analysis has shown. In order to decrease the weight and increase the chance of having a successful pod, the option of downsizing the fan or eliminating it altogether will be explored. With a decrease in weight the potential accelerations will increase, the quantity of levitation motors will decrease and the end cost of the pod will decrease making it more feasible. Figure 54 shows the first revision of the new frame design, a simpler and smaller frame that will decrease the final weight of the pod.

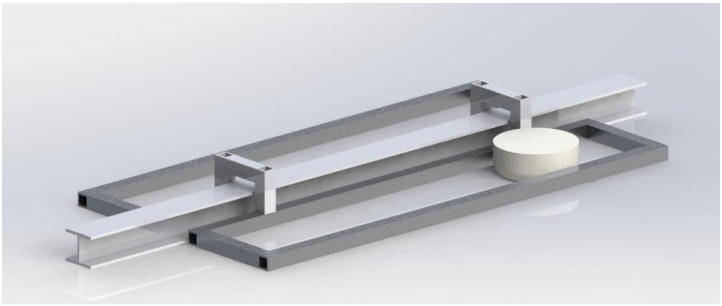

Figure 54. New Frame Design

This new frame design uses 2x2 in. 6061 aluminum tubing, with a 1/4 in. wall. The frame will be welded and used to mount the 4 motors, fan and additional components, including the carbon fiber body. Table 14 shows a comparison with the old design and new design. The Carbon fiber body weight and cost was estimated using .01 in. thick carbon fiber over the surface area of a cylinder with 3ft radius and 6ft height.

Table 14. Comparison with old and new design

	Old Design	**New Design**
Weight	1,150 lbs	390 lbs
Arx Pax Requirement	8	4
Power Requirement	44.5 kW	26.4 kW
Final Cost	$41,531	$29,131

Initial FEA has been performed on this new frame to ensure structural integrity is not sacrificed. Figure 55 shows the FEA and the critical points. These critical points will be further analyzed to ensure that they are reinforced. The FEA of the new frame shows that it is below yield and that the frame can be minimized. The FEA was perform by setting fixed boundary conditions at the eight corners of the frame. A force of 600 lbs is applied to the four split planes where the levitation motors will be acting.

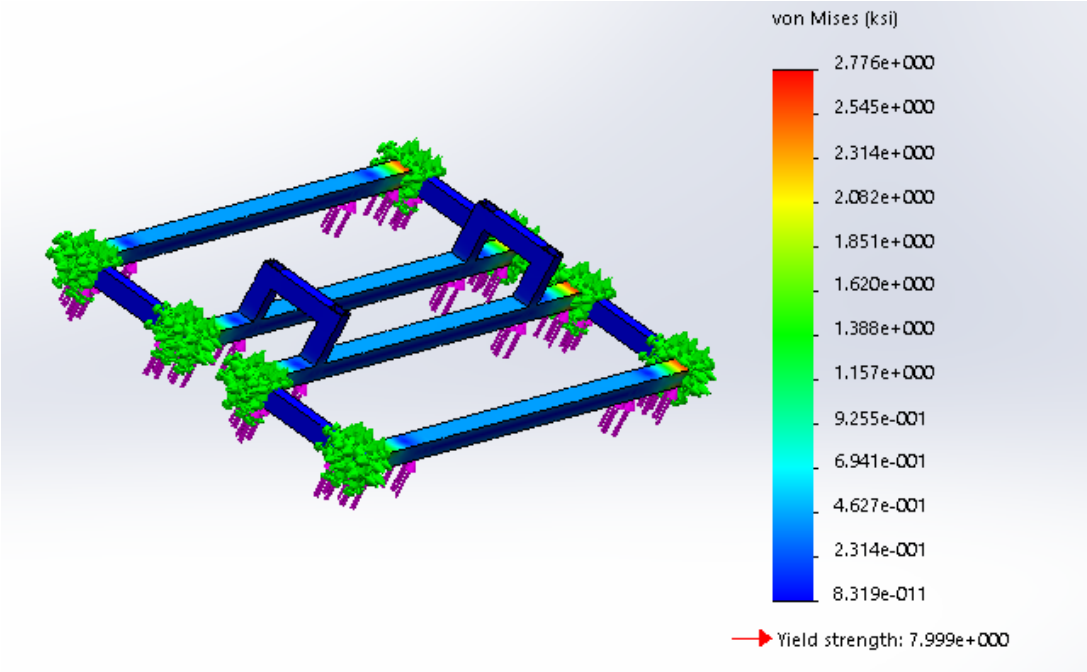

Figure 55. FEA on New Frame Design

18 TABLE OF FIGURES & TABLES

Table of Figures

Table of Tables

19 REFERENCES

3/8" Clear Vinyl Tubing. *Digital image*. RSA. N.p., n.d. Web. 14 Oct. 2015.

"Air Bearing Application and Design Guide." *New Way Air Bearings* E (2006): n. pag.Newwayairbearing.com. *New Way Air Bearing*. Web. 14 Oct. 2015.

Air Bearing Design. Digital image. *Coordinate Measuring Machine*. N.p., n.d. Web. 14 Oct. 2015.

“ALU-DRY Technology”. ACS. Digital Image.N.p.,n.d. Web 13 Oct 2015.

"Aluminum Alloys in Aviation." *Experimental Aircraft*. N.p., n.d. Web. 16 Oct. 2015.

Analog Devices Inc. Understanding How a Voltage Regulator Works. Norwood: Analog Devices Inc., 2009. PDF.

Chin, Jeffrey C. "Open-Source Conceptual Sizing Models for the Hyperloop Passenger Pod." (n.d.): n. pag. NASA Glenn Research Center. Web. 14 Oct. 2015.

"Control Systems." *MATLAB & Simulink Solutions*. Mathworks, n.d. Web. 18 Sept. 2015.

"Design Analysis of the Zeke 32." *Rwebs.net*. Ed. Leslie E. Neville. Aviation Magazine, n.d. Web. 15 Oct. 2015.

"DueMotorShieldDC." *Arduino Tutorials*. Arduino, n.d. Web. 18 Sept. 2015.

"Fluid Mechanics and Thermodynamics of Turbomachinery", S. L. Dixon and C. A. Hall, 2010, Hall, 6th ed.

Jeffrey C. Chin, Justin S. Gray, Scott M. Jones, Jeffrey J. Burton. “Open-Source Conceptual Sizing for the Hyperloop Passenger Pod.” Oct 14 2015.

Ling, A. L., and Viska Mulyandasari. "Compressor Selection and Sizing." *Practical Engineering Guidelines for Processing Plant Solutions* 2 (2011): n. pag. *KLM Techology Group*. KLM, Jan. 2011. Web. 18 Sept. 2015.

"Material Data Sheet." ASM. N.p., n.d. Web. 16 Oct. 2015.

NewMar Telecom. Circuit Breaker Distribution Panel. Newport Beach: NewMar Telecom, May 2015. PDF.

Musk, Elon. *Hyperloop Alpha*. Tech. no. 20130812. SpaceX, 13 Aug. 2013. Web. 27 May 2015.

"OAV Air Bearings." *OAV Air Bearings*. N.p., n.d. Web. 14 Oct. 2015.

Optima Batteries Inc. YELLOWTOP Specification Sheet. Milwaukee: Optima Batteries Inc., Dec. 2008. PDF.

"Patent US20130043346." *Google Books.* N.p., n.d. Web. 16 Oct. 2015.

"Predicting Post-Buckling Response and Ultimate Failure of Composite 2-Stringer Panels."*GENOA Engineering Newsletter*. N.p., 10 July 2008. Web. 16 Oct. 2015.

“Real World Best Practices”. Exair. Web 14 Oct 2015.

"Rolling Resistance." Engineering Toolbox. N.p., n.d. Web. 14 Oct. 2015.

“Sizing an Air Receiver”. Engineering Toolbox. Digital Image.N.p.,n.d. Web 13 Oct. 2015.

STMicroelectronics. Positive Voltage Regulators. Geneva: STMicroelectronics, 2010. PDF.

"Top Ten Fastest Trains in the World." - Railway Technology. Railway Technology, 29 Aug. 2013. Web. 13 Oct. 2015.

Turna, Onur. "Pure Sine vs. Modified Sine Wave Inverters." CivicSolar. CivicSolar, 08 Apr. 2011. Web. 25 Nov. 2015.

Vuchic, Vukan R,, and Jeffrey M. Casello. "An Evaluation of Maglev Technology and Its Comparison with High Speed Rail." *Transportation Quarterly* 56.2 (2002): 33-49. Penn Engineering. *Penn State.* Web. 14 Oct. 2015.

Xantrex Technology Inc. PROwatt SW Sine Wave Inverters. Burnaby: Xantrex Technology Inc., 2009. PDF.

20 ACKNOWLEDGMENTS

Ron Rorrer, Faculty Adviser

Doug Gallagher, Faculty Adviser

Joseph Cullen, Wind Tunnel Testing

Dana Carpenter, 3D Model Printing

Max Hazelrigg, 3D Renderings

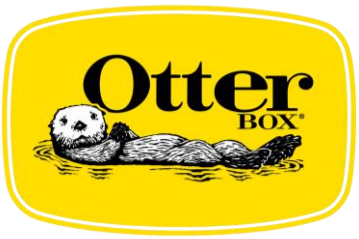

21 REVISION HISTORY

Revision 1 (12/1/2015 2:25AM)

Compiled: Fan & Propulsion, Frame & Body, Introduction, Levitation, Pod Free Body Diagram, Pod Weight.

Revision 2 (12/1/2015 5:54PM)

Changed CFD figures in aero section

Added budget, community outreach and fundraising and path forward/recommendation slides

Revision 3 (12/1/2015 5:07PM)

Added power and competition guidelines. Edited aero/frame/body